Am J Physiol Gastrointest Liver Physiol 324: G262–G280, 2023.
First published February 7, 2023; doi:10.1152/ajpgi.00251.2022

american physiological society

AMERICAN JOURNAL OF PHYSIOLOGY
GASTROINTESTINAL AND LIVER PHYSIOLOGY

RESEARCH ARTICLE

Deconstructing Organs: Single-Cell Analyses, Decellularized Organs, Organoids, and Organ-on-a-Chip Models

A leaky human colon model reveals uncoupled apical/basal cytotoxicity in early *Clostridioides difficile* toxin exposure

Meryem T. Ok,[1]* Jintong Liu,[2]* R. Jarrett Bliton,[1] Caroline M. Hinesley,[2] Ekaterina Ellyce T. San Pedro,[2] Keith A. Breau,[3] Ismael Gomez-Martinez,[3] Joseph Burclaff,[1,2] and Scott T. Magness[1,2,3,4]

[1]*Joint Department of Biomedical Engineering, University of North Carolina at Chapel Hill and North Carolina State University, Chapel Hill, North Carolina, United States;* [2]*Center for Gastrointestinal Biology and Disease, University of North Carolina at Chapel Hill and North Carolina State University, Chapel Hill, North Carolina, United States;* [3]*Department of Cell Biology and Physiology, University of North Carolina at Chapel Hill, Chapel Hill, North Carolina, United States; and* [4]*Department of Medicine, University of North Carolina at Chapel Hill, Chapel Hill, North Carolina, United States*

Abstract

Clostridioides difficile (*C. difficile*) toxins A (TcdA) and B (TcdB) cause antibiotic-associated colitis in part by disrupting epithelial barrier function. Accurate in vitro models are necessary to detect early toxicity kinetics, investigate disease etiology, and develop preclinical models for new therapies. Properties of cancer cell lines and organoids inherently limit these efforts. We developed adult stem cell-derived monolayers of differentiated human colonic epithelium (hCE) with barrier function, investigated the impact of toxins on apical/basal aspects of monolayers, and evaluated whether a leaky epithelial barrier enhances toxicity. Single-cell RNA-sequencing (scRNAseq) mapped *C. difficile*-relevant genes to human lineages. Transcriptomics compared hCE to Caco-2, informed timing of in vitro stem cell differentiation, and revealed transcriptional responses to TcdA. Transepithelial electrical resistance (TEER) and fluorescent permeability assays measured cytotoxicity. Contribution of TcdB toxicity was evaluated in a diclofenac-induced leaky gut model. scRNAseq demonstrated broad and variable toxin receptor expression. Absorptive colonocytes in vivo displayed increased toxin receptor, Rho GTPase, and cell junction gene expression. Advanced TcdA toxicity generally decreased cytokine/chemokine and increased tight junction and death receptor genes. Differentiated Caco-2 cells remained immature whereas hCE monolayers were similar to mature colonocytes in vivo. Basal exposure of TcdA/B caused greater toxicity and apoptosis than apical exposure. Apical exposure to toxins was enhanced by diclofenac. Apical/basal toxicities are uncoupled with more rapid onset and increased magnitude postbasal toxin exposure. Leaky junctions enhance toxicity of apical TcdB exposure. hCE monolayers represent a physiologically relevant and sensitive system to evaluate the impact of microbial toxins on gut epithelium.

NEW & NOTEWORTHY Novel human colonocyte monolayer cultures, benchmarked by transcriptomics for physiological relevance, detect early cytopathic impacts of *Clostridioides difficile* toxins TcdA and TcdB. A fluorescent ZO-1 reporter in primary human colonocytes is used to track epithelial barrier disruption in response to TcdA. Basal TcdA/B exposure generally caused more rapid onset and cytotoxicity than apical exposure. Transcriptomics demonstrate changes in tight junction, chemokine, and cytokine receptor gene expression post-TcdA exposure. Diclofenac-induced leaky epithelium enhanced apical exposure toxicity.

absorptive colonocyte monolayers; intestinal stem cells; permeability; toxicity

INTRODUCTION

Clostridioides difficile is a toxin-producing bacterium that causes *C. difficile* infection (CDI), with symptoms ranging from mild diarrhea to severe colitis and associated with life-threatening illnesses such as toxic megacolon and bowel perforation (1). CDI has a tremendous economic burden, costing an estimated $6.3 billion in annual healthcare expenses in the United States alone (2). Patients with greater CDI risk include those who are immunocompromised, receiving broad-spectrum antibiotics, or battling a leaky gut, often due to underlying chronic illness such as inflammatory bowel disease (IBD) (2, 3). Although fidaxomicin and vancomycin remain first-line antibiotics for patients with CDI, the high treatment costs (4), emergence of antibiotic-resistant strains (5), and increase in recurrence rates (6)

*M. T. Ok and J. Liu contributed equally to this work.
Correspondence: S. T. Magness (magness@med.unc.edu).
Submitted 25 October 2022 / Revised 31 January 2023 / Accepted 5 February 2023

especially for hypervirulent strains (≥23%) (6, 7) are growing problems.

C. difficile damages the colonic epithelium by secreting Toxin A (TcdA), Toxin B (TcdB), and binary toxin *C. difficile* transferase (CDT). CDT is produced by ~20% of *C. difficile* strains, but it receives less clinical attention given that CDT-producing strains lacking TcdA and TcdB are nontoxigenic in vitro (8, 9). TcdA and TcdB (TcdA/B) are homologous glucosyltransferases that bind to various host cell receptors, enter cells via endocytosis, and inactivate Rho-family GTPases by monoglucosylation (10). This ultimately results in cytoskeletal disassembly, tight junction collapse, cytopathic cell rounding, and eventual apoptosis (11–15). Although the TcdA/B receptor distribution likely impacts the onset of cytopathic events, this distribution has not been thoroughly mapped across the proximal-distal axis of the human gut or across epithelial cell lineages. A comprehensive map of *C. difficile* toxin receptors across all undifferentiated and differentiated lineages would address a major gap in knowledge and serve as a foundation to better understand mechanisms of toxin interactions with the epithelium, disease onset, progression, and resolution.

Alternatives to antibiotic therapies are becoming an attractive approach to treat CDI; however, physiologically relevant preclinical models of the human colon to test new therapies are lacking. Historically, *C. difficile* toxicity models relied on nonintestinal cell types (e.g., Vero, HeLa) or colon cancer cell lines (e.g., T84, HT-29, Caco-2) (16–19). However, colon cancer cells do not express physiological transporters/carriers found in healthy human colonic epithelium (hCE), and they phenotypically resemble small intestinal enterocytes (20, 21). Although TcdB is more cytotoxic than TcdA in T84 cells and nonintestinal epithelium (22, 23), TcdA is more potent than TcdB in three-dimensional (3D) human intestinal organoids (HIOs) and jejunal enteroid-derived monolayers (24, 25). Although a significant improvement in physiological accuracy, 3D organoids, in which the apical cell surface faces inward inside an enclosed epithelium, do not allow easy simultaneous access to apical/basal cell surfaces to apply toxins or assess barrier function using transepithelial electrical resistance (TEER) or permeability assays. Moreover, HIOs are induced to differentiate from pluripotent stem cells in vitro, and the resulting organoids are more similar to fetal small intestine (26) than colon, which is the predominant site of CDI (27), giving these findings limited generalizability to the sensitivity of adult differentiated hCE to TcdA/B. Thus, more physiologically accurate culture systems are essential to mimic in vivo colonic epithelium and investigate the impact of TcdA/B on hCE.

Currently, there are no established quantitative culture systems that simultaneously evaluate the apical versus basal impact of TcdA/B on hCE. *C. difficile* toxins are secreted in the lumen and thought to interact first with the apical aspect of the intestinal or colonic epithelial barrier (28). However, receptor studies in colon cancer cell lines (28, 29) and in nonhuman, nonintestinal epithelial cells (30) reveal that some TcdA receptors locate to the basal side of the cell, making them inaccessible to TcdA when there is an intact physiological epithelial barrier. This raises the possibility that a healthy epithelial barrier may be more refractory to apical TcdA cytotoxicity than previously believed, but this has yet to be tested in hCE. Likewise, although some TcdB receptors localize to the basal aspect of the epithelium (31–33), their full apical/basal distribution remains unclear (34, 35), though functional studies in HIOs show distinct apical and basal differences in barrier disruption (24). Thus, we designed a model to quantify the magnitude and time course of apical/basal toxicity, which could inform whether early clinical interventions should target apical versus basal hCE.

Here, we establish a physiologically relevant in vitro model of *C. difficile* TcdA/B toxicity using primary adult intestinal stem cell (ISC)-derived hCE monolayers. Building on our previous methods of culturing primary ISCs from healthy human donor organs and differentiating these ISCs into a functional epithelial layer (36–38), we develop a highly sensitive assay system for evaluating early-stage intestinal barrier injury and late-stage cytotoxic events associated with TcdA/B. Our tissue engineering approach focuses on producing an epithelium that closely mimics in vivo colonic tissue, which we use to assess *C. difficile*-relevant transcriptional and phenotypic differences between hCE, human small intestinal epithelium (hSIE), and Caco-2 cells. Using this system, we test the temporal dynamics of apical and basal TcdA/B toxicity, measure the effect of a leaky epithelium on toxin activity, and present biological insights into the impact of apical and basal cytotoxicity of TcdA/B.

METHODS

Donor Selection

Human transplant-grade donor intestines were obtained from HonorBridge (Durham, NC) and exempted from human subjects research by the UNC Office of Human Research Ethics. Donor acceptance criteria were as follows: age 65 yr or younger, brain-dead only, negative for human immunodeficiency virus, hepatitis, syphilis, tuberculosis, or COVID-19, as well as no prior history of severe abdominal injury, bowel surgery, cancer, or chemotherapy. Pancreas transplant donors were also excluded due to excision of proximal small intestinal tissue. Human intestinal tissue from three male donors (aged 29, 45, and 53 yr) was used for scRNAseq (39). Colonic tissue from a 34-yr-old Hispanic male was used for bulk RNAseq, immunofluorescence staining, and monolayer studies involving FITC-conjugated dextrans. Tissue from the same donor, in addition to tissue from a 51-yr-old African American male and a 29-yr-old White male, was used for TcdA and TcdB apical versus basal cell surface studies comparing colon and small intestine.

Single-Cell RNA-Sequencing Processing and Analysis

Single-cell data were obtained from our previously published human intestinal data set (Gene Expression Omnibus accession number: GSE185224), sequenced using an Illumina NextSeq 500 (Illumina, San Diego, CA) (39). All processing and analyses were completed using scanpy (v1.7.2) (40). Read counts were normalized to the median read depth of the data set and log-transformed.

Bulk RNA-Sequencing Preparation, Processing, and Analysis

To examine the changes in gene expression as colon stem cells differentiate into late absorptive colonocytes (ACCs) in vitro, RNAseq was performed on hCE monolayers that were

harvested the day after seeding onto Transwells [expansion media (EM) *day 1*], immediately before switching to differentiation medium (DM; *day 0*), and on *days 2* and *4* of differentiation on Transwells. For Caco-2, RNAseq was performed using cells harvested on *day 22* of differentiation. To evaluate the impact of apical 1× TcdA on gene expression of tight junctions as well as cytokines and their receptors, RNAseq was performed on differentiated hCE monolayers after 8- or 20 h of toxin exposure. Three technical replicates were collected at each time point, and RNA was extracted via the RNAqueous-Micro Total RNA Isolation Kit (AM1931; ThermoFisher, Waltham, MA) according to the manufacturer's protocol.

Before cDNA library preparation, RNA quality was determined by quantifying RNA integrity number (RIN), the ratio of 28s/18s RNA present, and RNA concentration in each sample. All samples used in library preparation had a RIN of at least 7. RIN was determined with the RNA 6000 Pico Kit for the Agilent 2100 Bioanalyzer. The Advanta RNA-Seq NGS Library Prep Kit for the Standard BioTools (formerly Fluidigm) Juno was used to prepare cDNA libraries for sequencing. Bulk sequencing was run on a NovaSeq 6000 instrument using one lane of an S4 v1.5 flow cell (Illumina), 2B paired-end reads, 150× read length. The Kallisto package was used to quantify transcript abundance, which were pseudoaligned to human genome GRCh38. The output gene expression matrix was normalized using TMM normalization. Principal component analysis was performed with scikitlearn (v0.24.0, Rocquencourt, France) (41). Differential gene expression analysis following toxin exposure was performed with DESeq2 on non-TMM normalized gene counts (42). Gene set enrichment analysis (GSEA) was performed with normalized bulk RNAseq data using GSEA v4.2.3 (43, 44) and previously published gene signatures for colon ISC and late ACC clusters versus the rest of the colon (39). Data will be available in the NCBI Gene Expression Omnibus, accession number: GSE223605.

Collagen Hydrogel Scaffold Preparation

Six-well tissue-culture plates (3516; Corning, Corning, NY) for expansion were coated with ice-cold type I rat-tail collagen (354236; Corning, Corning, NY) in neutralization buffer based on an established protocol (45). Briefly, after being incubated at 37°C in 5% CO_2 for 1 h, sterile tissue-culture plates were coated with 1 mL of diluted (1 mg/mL) rat-tail collagen for each well. Plates were incubated at 37°C in 5% CO_2 for 1 h, then 3-mL room temperature 1× Dulbecco's phosphate-buffered saline (DPBS) (14040141; Thermo Fisher Scientific, Waltham, MA) was added onto each well. Plates were then kept overlaid with DPBS at room temperature for ≥2 wk before use.

Primary Human Crypt Isolation and Intestinal Epithelial Stem Cell Culture

Surgical specimens of human small and large intestines were obtained from donors at HonorBridge (formerly Carolina Donor Services, Durham, NC). Crypts from desired regions (Jej, DC) of each donor were detached from the specimen as previously described (36, 37, 39) using a chelating buffer (46) composed of EDTA (2 mM), dithiothreitol (DTT, 0.5 mM, freshly added), Na_2HPO_4 (5.6 mM), KH_2PO_4 (8.0 mM), NaCl (96.2 mM), KCl (1.6 mM), sucrose (43.4 mM), D-sorbitol (54.9 mM), pH 7.4. Released crypts were expanded as a monolayer on a neutralized collagen hydrogel as described previously (36–38).

Briefly, crypts were placed on the top of 1 mg/mL collagen hydrogels (1 mL into each well of 6-well plate) at a density of 10,000 crypts/well, overlaid with 3 mL of expansion media (EM) containing 10 mmol/L Y-27632 (S1049; SelleckChem, Houston, TX), and incubated at 37°C in 5% CO_2. See Table 1 for small intestine and colon EM formulations. EM was used to expand the epithelial cell numbers as monolayers; media was changed the day after seeding and every 48 h afterward. When the cell coverage was greater than 80% (typically 4–6 days), the epithelium was dissociated to fragments to seed onto either 6-well tissue-culture plates coated with collagen hydrogels for continued expansion, or onto 12-well Transwell inserts (3460; Corning, Corning, NY) coated with 1% Matrigel for experiments.

Transwell Preparation and Intestinal Epithelial Stem Cell Differentiation

Briefly, 500-μL ice-cold 1% Growth Factor Reduced Matrigel (354230; Corning, Corning, NY) diluted in ice-cold DPBS was added to the apical surface of 12-well Transwell inserts. Transwell plates were then incubated at 37°C in 5% CO_2 overnight and then rinsed 2–3 times with 1× DPBS. Dissociated intestinal epithelial stem cells that were expanded on collagen hydrogels were resuspended in 500 μL of EM per Transwell insert and seeded on the apical surface of each insert at an approximate density of 1.5×10^5 cells/cm^2. EM (1.5 mL) was added to the basal reservoir at the time of seeding. Both the apical and basal media were replaced with fresh EM the day after seeding. After sufficient cell coverage on Transwells (e.g., no visible monolayer gaps), on *day 4*, differentiation medium (DM) (47) (Table 1) was used to initiate differentiation as well as during toxin experiments.

Caco-2 Cell Culture and Differentiation

Caco-2 cells (HTB-37; ATCC, Manassas, VA) were grown on a 10-cm polystyrene tissue-culture-treated dish (430167; Corning, Corning, NY) in Dulbecco's Modified Eagle Media + 10% fetal bovine serum + 1% penicillin-streptomycin based on an established protocol (Table 2) (48). Caco-2 media was changed every 2 days until desired confluency was reached. Two 60% confluent 10-cm dishes were seeded onto 24 inserts in 12-well Transwell plates coated with 30 μg/mL collagen in 1× DPBS. Spontaneous differentiation of Caco-2 monolayers was allowed to occur over 22 days, and media was changed every 2 days until the start of toxin experiments on *day 22*.

C. difficile Toxins Information

Toxin A (SML1154; Sigma-Aldrich, St. Louis, MO) and Toxin B (SML1153; Sigma-Aldrich, St. Louis, MO) were reconstituted in purified water and then diluted to 30, 150, or 300 pM (for dose-response) in DM before adding to differentiated cells or Caco-2 on Transwell plates. These native toxins are purified from *C. difficile* strain VPI10463 (toxinotype 0), which is from Clade 1 (as opposed to Clade 2 strains for which TcdB does not appear to bind FZDs) (49). 30 pM (1×)

Table 1. *Formulations of primary cell culture media*

Component	Stock Concentration	Vendor/Cat. No.	Volume Required for 500 mL (Final Concentration)		
			EM (Small Intestine)	EM (Colon)	DM
L-WRN conditioned medium[a]	N/A	N/A	250 mL (50%, vol/vol)	250 mL (50%, vol/vol)	
Adv. DMEM/F12	1×	ThermoFisher, 12634010	225 mL (45%, vol/vol)	230 mL (46%, vol/vol)	490 mL (98%, vol/vol)
GlutaMAX	100×	ThermoFisher, 35050061	2.5 mL (1×)[b]	2.5 mL (1×)[b]	5 mL (1×)
HEPES	1 M	Corning, 25-060-CI	5 mL (10 mM)	5 mL (10 mM)	5 mL (10 mM)
Primocin	50 mg/mL	Invivogen (VWR), mspp-ant-pm2	500 µL (50 µg/mL)	500 µL (50 µg/mL)	500 µL (50 µg/mL)
Pen/strep	100×	ThermoFisher 15070063	2.5 mL (1×)[b]	2.5 mL (1×)[b]	
N-acetylcysteine	500 mM	Sigma-Aldrich, A9165	1.25 mL (1.25 mM)	1.25 mL (1.25 mM)	1.25 mL (1.25 mM)
EGF, murine	1 mg/mL	Peprotech, 315-09	25 µL (50 ng/mL)	25 µL (50 ng/mL)	25 µL (50 ng/mL)
Nicotinamide	1 M	Sigma-Aldrich, N0636	5 mL (10 mM)		
B27 Supplement	50×	ThermoFisher, 12587001	10 mL (1×)	10 mL (1×)	
Gastrin	100 µM	Sigma-Aldrich, G9145	50 µL (10 nM)	50 µL (10 nM)	
Prostaglandin E2	1 mM	Peprotech, 3632464	5 µL (10 nM)		
A 83-01	500 µM	Sigma-Aldrich, SML0788		500 µL (500 nM)	500 µL (500 nM)
SB202190	30 mM	Peprotech, 1523072	50 µL (3 µM)	50 µL (3 µM)	
Y-27632	10 mM	Selleck Chemical, S6390	500 µL (10 µM)	500 µL (10 µM)	
Fetal bovine serum	N/A	VWR, 97068-085	0 mL (10%, vol/vol)[b]	0 mL (10%, vol/vol)[b]	

[a]Prepared by culture of L-WRN cell line (ATCC, CRL-3276) and harvesting medium containing Wnt3a, R-spondin 3, and noggin. [b]Final concentration reflects ~1:1 mixture with L-WRN conditioned media, which contains adv. DMEM/F12 (78% vol/vol), fetal bovine serum (20% vol/vol), GlutaMAX (1×), and pen/strep (1×). No additional FBS is added to EM. DM, differentiation media; EM, expansion media.

was chosen as a clinically relevant concentration based on ultrasensitive digital enzyme-linked immunosorbent assays (ELISAs) for TcdA and TcdB conducted on clinical specimens that tested positive for cytotoxicity (50).

Transepithelial Electrical Resistance Measurements

Intestinal epithelial barrier integrity was quantified via transepithelial electrical resistance (TEER) using an EVOM2 paired with STX2 electrodes (World Precision Instruments). TEER was measured daily during differentiation and every 2 h after adding toxin for 12 h, followed by a 24-h time point. Toxin was added on DM *day 3* (DC) or DM *day 4* (jejunum). For Caco-2, TEER was measured every two days (starting *day 1*) and media was changed every 2 days during spontaneous differentiation. For Caco-2 TEER measurements in the presence of toxin, TcdA or TcdB was added to the apical or basal side of Transwell inserts on *day 22*.

Genetically Engineering an EGFP-ZO-1 Tight Junction Reporter in Human Colonic Epithelium

Genetic engineering of the EGFP-ZO-1 reporter was performed using previously established methods (37, 51). Briefly, DNA segments of interest were amplified using CloneAmp HiFi PCR Premix (639298; Takara Bio USA, San Jose, CA) or isolated using restriction enzymes. Plasmids were assembled using an In-Fusion HD Cloning Kit (102518; Takara Bio USA, San Jose, CA) and amplified/isolated from bacterial stocks using a HiSpeed Plasmid Maxi Kit (12662; QIAGEN, Hilden, Germany). The plasmid pEGFP ZO1 was used to generate the EGFP-ZO-1 reporter and was a gift from Alan Fanning (Addgene plasmid No. 30313; http://n2t.net/addgene: 30313; RRID:Addgene_30313) (52).

The EGFP-ZO-1 plasmid was then electroporated into human colonic ISCs using the Neon Transfection System 100-µL Kit (MPK10096; ThermoFisher, Waltham, MA). Cells were resuspended in 100 µL of Neon Buffer R at 10,000 cells/µL with 6 µg of EGFP-ZO-1 plasmid and 5 ng/µL of Super PiggyBac Transposase Expression Vector (PB210PA-1; System Biosciences, Palo Alto, CA). Neon preset no. 5 (1,700 V, 1 pulse, 20 ms) was used to electroporate cells, which were then immediately added to a 6-well collagen hydrogel-coated plate with 3-mL EM + 1:1,000 Y-27632. Colonies were selected using 6.6 µg/mL Blasticidin for 1 wk and isolated by digesting the collagen hydrogel with 5,000 U/mL collagenase IV at 100 µL/mL at 37°C for 25 min. After colonies were washed with 1× DPBS, individual colonies were picked using a 20-µL pipette and light microscope and plated in individual wells of a 96-well collagen-coated plate with 100 µL of EM + 1:1000 Y-27632. Once confluent, cells were expanded up for eventual expansion on 6-well collagen-coated plates.

Microscopy and Immunofluorescence Staining of Human Colonic Epithelium

Human colonic EGFP-ZO-1 reporter cells were plated onto a 24-well collagen-coated plate in EM and fixed in 4% paraformaldehyde in PBS at 37°C for 15 min after 2 days of expansion. Cells were then permeabilized in 0.5% Triton-X100 at room temperature for 20 min, followed by blocking with 3% BSA in 1× DPBS for 1 h at room temperature. The cells were treated with primary antibody against ZO-1 (1:2000, 21773-1-AP;

Table 2. *Formulation of Caco-2 media*

Component	Stock Concentration	Vendor/Cat. No.	Volume Required for 500 mL (Final Concentration)
DMEM	1×	ThermoFisher, 11995065	445 mL (89%, vol/vol)
Fetal bovine serum	N/A	VWR, 97068-085	50 mL (10%, vol/vol)
Pen/strep	100×	ThermoFisher, 15070063	5 mL (1×)

ProteinTech Group, Rosemont, IL) and incubated at 4°C overnight. The cells were then washed with a rinse solution consisting of 0.1% BSA, 0.2% Triton-X100, and 0.05% Tween-20, then incubated with Cy3-conjugated donkey anti-rabbit antibody (1:500, 711-166-152; Jackson ImmunoResearch, West Grove, PA) diluted in 3% BSA in 1× DPBS for 1 h at room temperature. Cells were washed in 1× DPBS twice before microscopy. Images were captured using a Keyence BZ-X800 microscope (Keyence; Osaka, Japan) ×40 objective, with postacquisition processing using FIJI (53). Differentiated EGFP-ZO-1 reporter hCE monolayers were fixed as above and imaged at indicated time points after apical addition of ×10 TcdA using an LSM700 confocal microscope (Zeiss, Jena, Germany) ×10 objective and ZEN 2011 acquisition software.

After the 24-h time point, control and TcdA- or TcdB-treated primary human colonic epithelial monolayers were fixed in 4% paraformaldehyde, permeabilized in 0.5% Triton-X100, and blocked with 3% BSA as above. The cells were treated with primary antibody against cleaved-caspase 3 (1:300, 9661S; Cell Signaling Technology, Danvers, MA) and incubated at 4°C overnight. The cells were then washed with a rinse solution consisting of 0.1% BSA, 0.2% Triton-X100, and 0.05% Tween-20 and then incubated with Alexa Fluor 488-conjugated donkey anti-rabbit antibody (1:500, 711-545-152; Jackson ImmunoResearch, West Grove, PA) and bisbenzimide H 33258 (1:1,000, B1155; Sigma-Aldrich-Aldrich, St. Louis, MO) diluted in 3% BSA in PBS for 1 h at room temperature. Cells were washed in 1× DPBS twice before microscopy. Images were captured using an LSM700 confocal microscope (Zeiss, Jena, Germany) ×10 objective and ZEN 2011 acquisition software, with postacquisition processing using FIJI (53).

Basal Fluorescent Dextran Quantification and Diclofenac Permeability Assays

Permeability assays were conducted as previously described (36). Briefly, 250 kDa FITC-Dextran (FD250S; Sigma-Aldrich, St. Louis, MO) was chosen to mimic the size of TcdB (270 kDa). FITC-Dextran was diluted to 1 μM in DM and added to the apical side of 12-well Transwell inserts with or without 30 pM TcdB. Basal media (100 μL) was collected every 2 h for 12 h and replaced with an equivalent volume of DM (or DM with TcdB), followed by a 24-h time point. Basal collections were added to a 96-well microplate for fluorescence-based assays (M33089; ThermoFisher, Waltham, MA). FITC-associated fluorescence was measured by CLARIOstar Plus Microplate Reader (BMG Labtech, Ortenberg, Germany) after excitation at 483 nm and detection at 530 nm. Relative fluorescence units were converted to picomoles using a standard curve. Diclofenac sodium salt (157660; MP Biomedicals, Solon, OH) was reconstituted in DMSO and diluted to 1 mM in DM containing FITC-Dextran with or without TcdB.

Statistics

For comparing gene expression in scRNAseq data, significance was calculated by negative binomial regression with the diffxpy python package (v0.7.4) using the Wald test and Benjamini-Hochberg correction. TEER values at each day of DM (or Caco-2 media) were compared against TEER at D0 (or Caco-2 *day 1*) using a one-way repeated-measures ANOVA with Bonferroni correction. Experimental TEER values were compared against vehicle control using a one-way ANOVA followed by Dunnett's multiple comparisons test. One-way ANOVA followed by Dunnett's multiple comparisons tests were used to compare FITC-Dextran permeability between control and experimental groups.

RESULTS

A Single-Cell Survey of Human Gut Epithelium Reveals Organ and Lineage Variability of *C. difficile* Toxin-Relevant Genes

Expression of *C. difficile*-relevant gene sets have not been characterized across the epithelial lineages of the small intestine and colon. To address this, we interrogated single-cell transcriptomic data across all lineages in small intestine and colon from three healthy human adult donors (Fig. 1*A*) (39) and evaluated the magnitude of toxin receptor expression (Fig. 1*B*) (28, 29, 31, 34, 54, 55). In general, the ISC, transit-amplifying (TA), and absorptive lineages in the small intestine and colon exhibited more toxin receptor expression and with higher magnitudes compared with the secretory lineages. Notably, follicle-associated epithelium (FAE) uniquely expressed high levels of the TcdB receptor *FZD7* (Fig. 1*B*). Lineage-specific *C. difficile* toxicities have not been evaluated; thus, these findings provide a foundation to investigate such questions.

Next, we sought to evaluate the *C. difficile*-relevant genes in the two key cell types involved in the initiation and resolution of *C. difficile* infections. The absorptive lineages are the predominant cell types in the small intestine and colon and experience first-line exposure to *C. difficile*, and the ISCs are responsible for regenerating the epithelium after damage. We surveyed curated gene sets for toxin receptor, Rho GTPase, and tight junction expression in ISCs and mature absorptive cells in six regions across the proximal-distal axis of the small intestine (Duodenum, Jejunum, Ileum) and colon (Ascending, Transverse, Descending; Fig. 2*A*). For the toxin receptor genes, sucrase-isomaltase is a small intestine-specific brush border enzyme (56); thus, it is not expected to be meaningfully expressed in the colon, as demonstrated by the data (Fig. 2*A*). When comparing the remaining receptors between small intestinal and colonic ISCs, there was no difference in *HSP90B1* and *LSR*, *FZD5* was significantly higher in colonic ISCs, and *LRP1* and *NECTIN3* were higher in small intestinal ISCs (Fig. 2*B*). In mature absorptive cells of the small intestine and colon, all receptors except for *LRP1* and small intestinal-specific *SI* were significantly higher in colon (Fig. 2*B*). For classic Rho-family GTPases (*CDC42*, *RAC1*, and *RHOA*) (57–59), which are terminal targets of *C. difficile* toxins, no specific gene demonstrated statistically significant differences between small intestinal and colonic ISCs (Fig. 2, *C* and *D*). However, in mature absorptive lineages, *RAC1* was modestly but significantly higher in small intestine, and *CDC42* and *RHOA* were higher in the colon (Fig. 2, *C* and *D*).

We analyzed tight junction proteins, which are known to be disrupted as a terminal effect of toxin-induced Rho GTPase glucosylation (14). A subset of 34 genes were selected from a published curated gene set based on classification of "tight junction" or "tight junction-associated" genes (60). Fifteen genes with the highest mean expression in mature

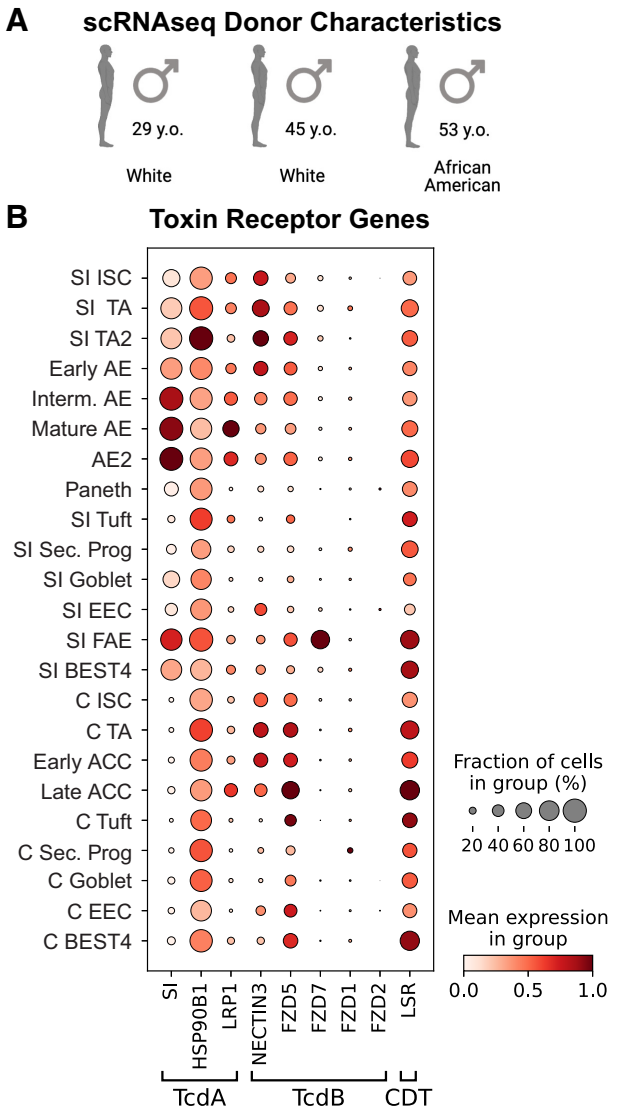

Figure 1. Single-cell transcriptomics demonstrates variations in expression patterns and magnitude of *Clostridioides difficile* toxin receptor genes across all intestinal epithelial cell lineages. *A*: healthy human organ donor demographic information for single-cell RNAseq data. *B*: dotplot showing the fraction of expressing cells (circle size) and magnitude (color) of expression for known *C. difficile* toxin receptor genes across all small intestinal and colonic epithelial cell lineages. ACC, absorptive colonocyte; AE, absorptive enterocyte; C, colon; EEC, enteroendocrine cell; FAE, follicle-associated epithelium; Interm., intermediate; ISC, intestinal stem cell; Sec. Prog, secretory progenitor; SI, small intestine; TA, transit-amplifying.

small intestinal and colonic absorptive lineages were grouped by transmembrane versus intracellular proteins and their expression was characterized across regions and lineages of the small intestine and colon (Fig. 2*E*). Claudin (*CLDN*) genes *CLDN3*, *CLDN4*, and *CLDN7*, which aid in forming selective barriers to macromolecules (such as *C. difficile* toxins) and ions (61), are highly expressed across all ISCs and mature absorptive cells, with notably higher expression in mature absorptive lineages of the colon (Fig. 2*F*). *CLDN15* showed unique and high expression in the ISCs and mature absorptive lineages of the small intestine. ISCs and mature absorptive lineages across all small intestinal and colonic regions demonstrated broad expression of the remaining tight junction genes, which were generally expressed at lower magnitude than the claudins (Fig. 2*F*). These findings highlight variability in small intestinal and colonic regions and lineages that could lead to functional differences in intestinal epithelial barrier function and likely influence CDI onset and progression.

Transcriptomics Show hCE Monolayers Mature over Time to Mimic In Vivo Mature Absorptive Colonocytes

With the single-cell transcriptomic data serving as the in vivo benchmark for physiological relevance, we sought to determine whether colonic ISCs could be differentiated in vitro to closely mimic the absorptive colonocytes in vivo. We also compared the transcriptomics of differentiated hCE monolayers with differentiated Caco-2 monolayers in an effort to establish which model more closely aligned to in vivo transcriptomic lineage states. To differentiate hCE monolayers, primary crypt-derived ISCs from the descending colon (DC) were first expanded on collagen-coated hydrogels as previously described (38). DC tissue was chosen given that CDI primarily manifests as colitis in the distal colon (27). Once confluent, these cells were then plated onto Matrigel-coated Transwell inserts in expansion media (EM) containing ISC growth factors (Wnt3a, R-spondin 3, and Noggin) for 4 days during which they continued to proliferate to form a confluent monolayer. To differentiate the colonic ISCs, differentiation media (DM) was applied to ISCs for an additional 4 days (Fig. 3*A*). RNA was isolated from hCE monolayers at various time points (EM *day 1*, EM *day 4* = DM *day 0*, DM *day 2*, and DM *day 4*), and transcriptomics was used to verify differentiation and characterize cell maturation.

Principal component analysis showed subtle transcriptomic changes while in EM (EM D1, DM D0) but substantial changes along principal component (PC) 1 and PC2 after 2 days of differentiation (DM D2), indicating large expression changes between *day 0* and *day 2* of colonic ISC differentiation (Fig. 3*B*). There were fewer transcriptomic changes between *day 2* and *day 4* of differentiation, indicating relatively stable transcriptomes during this time window. We compared hCE transcriptomics to 22-day differentiated Caco-2 cells to determine if Caco-2 transcriptomics tracked with differentiated hCE. Caco-2 cells were markedly separated from colonic ISCs and all stages of hCE differentiation in PC1, highlighting that differentiated Caco-2 monolayers are significantly different than the primary tissue-derived hCE monolayers (Fig. 3*B*).

We further characterized the differentiation of hCE monolayers at a more granular level to determine if time of differentiation could "mature" the monolayers to a transcriptomic state that resembles mature absorptive colonocytes in vivo. We curated two gene sets from the in vivo single-cell transcriptomic data as the standard for comparison, one from the colonic ISCs and one from the mature absorptive colonocytes (i.e., late ACCs) (39). The hypothesis was that replacement of EM with DM would shift the transcriptomic state of the monolayers away from the ISC signature and closer to the mature absorptive colonocyte signature. The data show that hCE monolayers at EM *day 1* are more closely aligned with the in vivo colonic ISC signature, but these similarities decrease over four days of differentiation where the magnitude of most

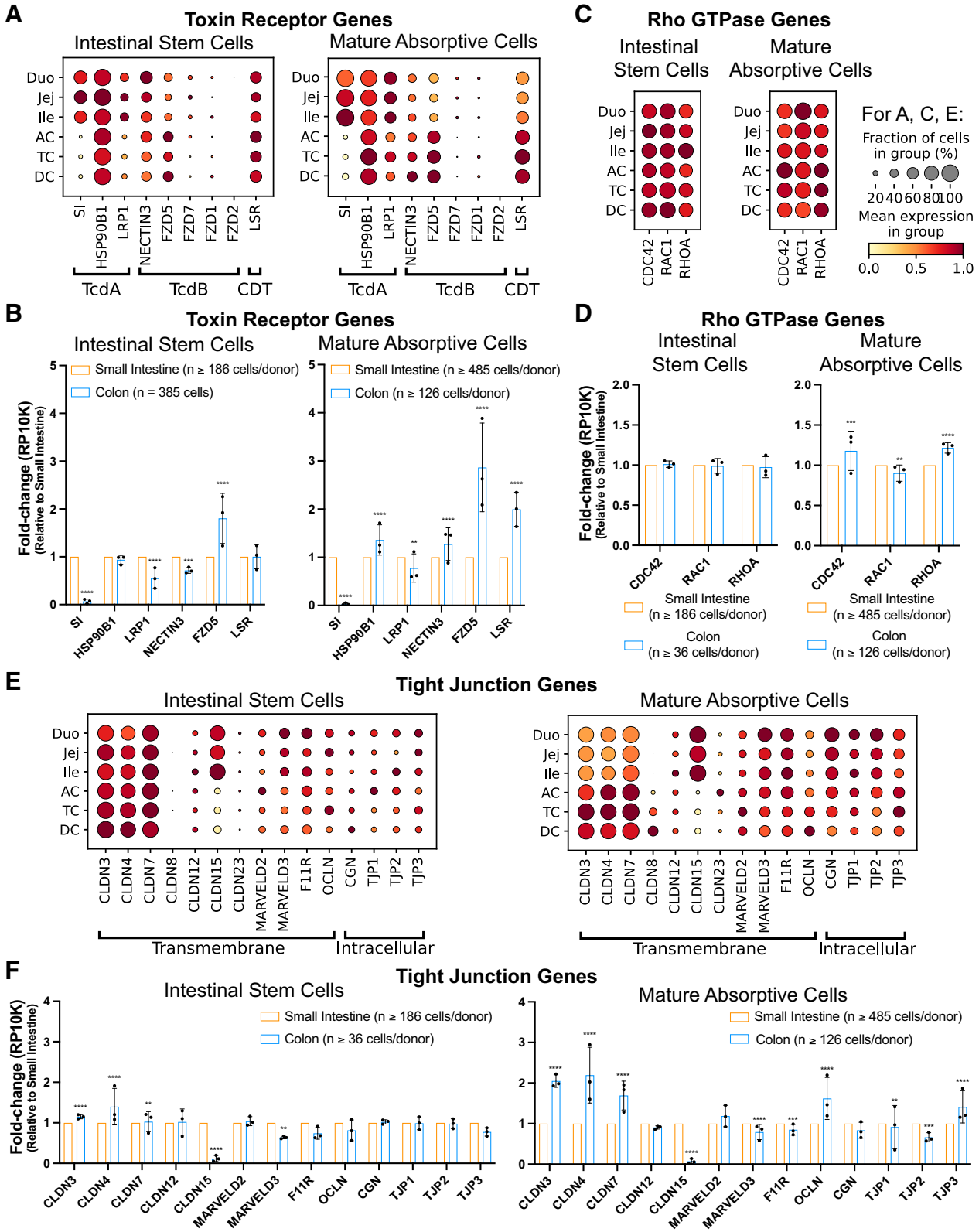

Figure 2. Single-cell RNAseq survey of *Clostridioides difficile* toxin-relevant genes reveals organ and lineage variability. Dotplots comparing *C. difficile* toxin receptor genes across small intestinal and colonic epithelial regions in stem cells (*left*) and mature absorptive cells (*right*; *A*) and corresponding significance bar graphs (*B*). Dotplots comparing Rho GTPase family genes by intestinal region in stem cells (*left*) and mature absorptive cells (*right*; *C*) and corresponding significance bar graphs (*D*). Dotplots comparing curated tight junction genes by intestinal region in stem cells (*left*) and mature absorptive cells (*right*; *E*) and corresponding significance bar graphs (*F*). All bar graphs show fold-change in reads per 10,000 genes (RP10K) across 3 donors for colon normalized to small intestine, means ± SD. *$q < 0.05$, **$q < 0.01$, ***$q < 0.001$, ****$q < 0.0001$. AC, ascending colon; DC, descending colon; Duo, duodenum; Ile, ileum; Jej, jejunum; TC, transverse colon.

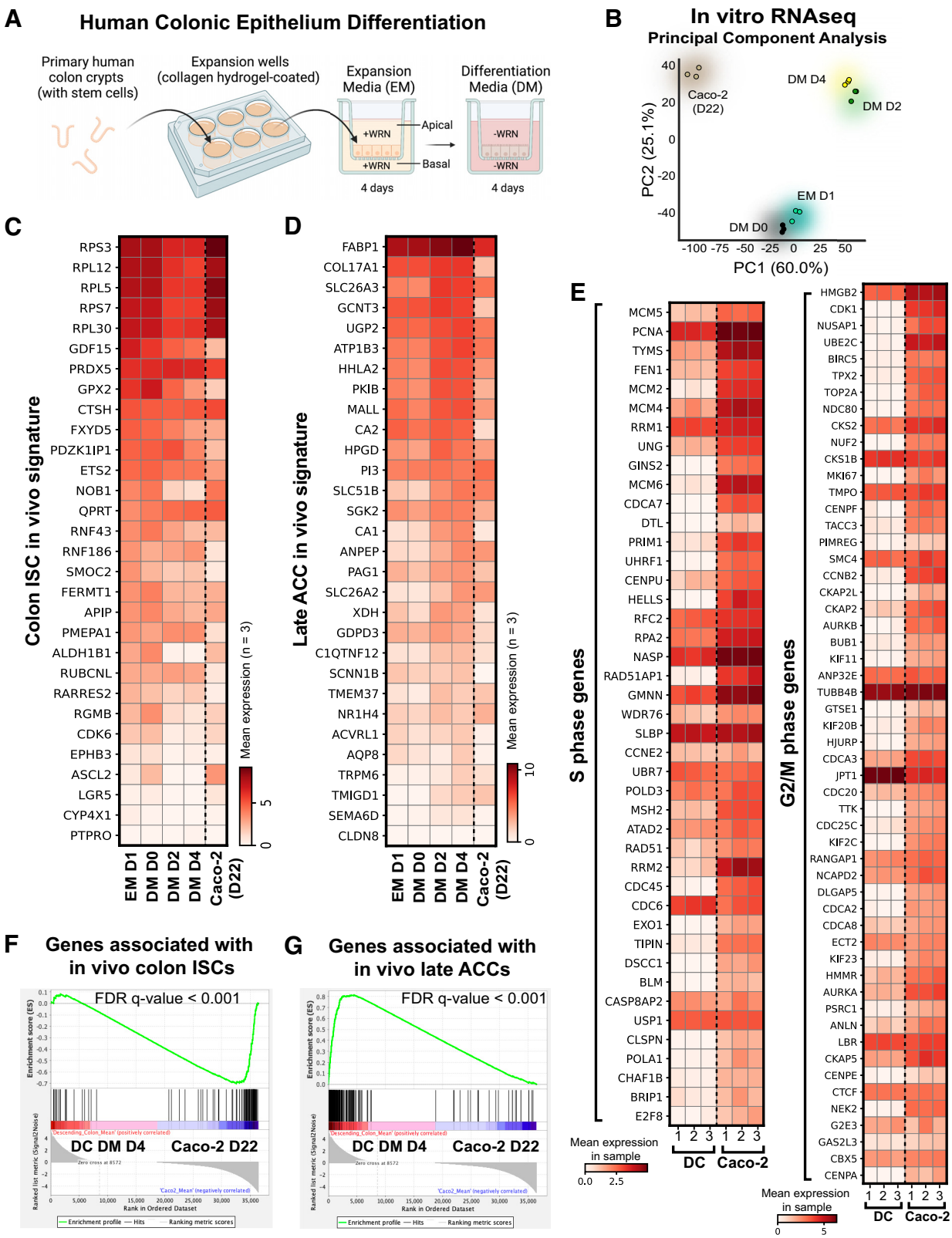

Figure. 3. Bulk RNAseq reveals Caco-2 monolayers remain stem-like and human colonic epithelial (hCE) monolayers mature over time to mimic in vivo late absorptive colonocytes. *A*: schematic of expansion and differentiation of human colonic epithelial (hCE) monolayers on Transwells. *B*: principal component analysis of sequenced transcriptomes. Matrix plots comparing hCE and Caco-2 cells ($n = 3$ Transwells each) using top 30 differentially expressed genes (DEGs) for (*C*) colon intestinal stem cells (ISCs) and (*D*) late absorptive colonocytes (ACCs) vs. the rest of the colon, and (*E*) S-phase and G2/M-phase genes in descending colon (DC) vs. Caco-2 cell monolayers. Gene set enrichment analysis for DC in differentiation media (DM) *day 4* (red) and differentiated Caco-2 cells (blue) using gene sets consisting of (*F*) all in vivo colon ISC DEGs and (*G*) all in vivo late ACC DEGs.

colonic ISC genes is reduced (Fig. 3*C*). By contrast, 22-day differentiated Caco-2 cells still exhibit higher expression of many colonic ISC genes, notably *LGR5* and *ASCL2* (Fig. 3*C*).

Conversely, when gene signatures of hCE and Caco-2 monolayers are compared with the in vivo late ACC signature, hCE cells show increased magnitude of gene expression at DM *day 2* which stabilized through DM *day 4* (Fig. 3*D*). In most instances, the 22-day differentiated Caco-2 genes more closely aligned with the expression patterns of EM *day 1* and DM *day 0*, which is reflective of a persistent undifferentiated state and further highlights the less mature state of differentiated Caco-2 cells (Fig. 3*D*). To characterize the extent of the undifferentiated state between differentiated hCE and Caco-2 monolayers, curated gene sets associated with S- and G2/M-phase cell cycle stages were analyzed (62). We hypothesized that differentiated hCE monolayers would express relatively lower levels of S- and G2/M-phase genes whereas Caco-2 monolayers would show upregulated expression of these genes. The data show that 22-day differentiated Caco-2 monolayers express higher levels of nearly all genes associated with cell cycling, notably the cell proliferation markers *MKI67* and *PCNA* (Fig. 3*E*). Finally, gene set enrichment analyses were performed using the full gene signature of in vivo colon ISCs (108 genes) and in vivo late ACCs (215 genes) (39). Consistent with our earlier observations, Caco-2 monolayers are significantly enriched for stem-like genes compared with hCE monolayers (Fig. 3*F*), whereas hCE monolayers are significantly enriched for late ACC genes compared with Caco-2 monolayers (Fig. 3*G*). These findings emphasize that hCE monolayers are more terminally differentiated and more aligned with the in vivo late ACC gene signature, which likely translates into better functional equivalence compared with Caco-2 cells.

Differentiated hCE Monolayers Exhibit Stronger TEER Barrier Properties than Caco-2 or hSIE Monolayers

Our findings point to substantial gene expression differences in lineage states between differentiated hCE and Caco-2 monolayers. Human small intestinal organoids and monolayers have been used to model TcdA/B toxicities; thus, we also compared barrier functions of hCE and hSIE monolayers. In prior work, we established a method for culturing healthy human jejunal monolayers and tracking cell maturation using transepithelial electrical resistance (TEER) (36), a noninvasive quantitative technique that is widely accepted to measure epithelial integrity (63). Here, we applied similar principles to differentiated hCE (DC), hSIE, and Caco-2 monolayers and characterized the variation in barrier properties as measured by TEER between multiple donors (Fig. 4*A*).

Daily TEER measurements were performed during monolayer expansion and differentiation (Fig. 4*B*). In hCE monolayers from three healthy human donors, TEER was measured for 4 days in EM followed by 4 days in DM (Fig. 4*C*). After just one day of DM exposure, hCE TEER reached an average value of 1,000–2,000 $\Omega \times cm^2$, consistent with a tight epithelial barrier (63). Although the individual TEER profiles varied by donor, the steep increase in hCE TEER after switching to DM was consistent across all three donors. It is noteworthy that both Caco-2 and hSIE monolayers did not reach high resistance like hCE cultures, with values staying below 500 $\Omega \times cm^2$ (Fig. 4, *D* and *E*). This finding is consistent with previous jejunal TEER studies even after 12 days of differentiation (36), supporting the notion that hCE monolayers have a different barrier strength profile than hSIE or Caco-2 monolayers, which exhibit lower barrier strength profiles. Thus, differentiated Caco-2 cells, which have a baseline TEER that is much lower than that of differentiated hCE and is more consistent with ISCs and hSIE, may not accurately report *C. difficile* toxin sensitivities in the colon.

Colonic Monolayers Exhibit a Dose-Dependent Early Cytotoxicity to TcdA after Apical Exposure

By *days 2–4* of differentiation, hCE monolayers show transcriptional signs of maturation (Fig. 3, *B* and *D*) and TEER is sufficiently elevated, indicating a tight barrier (Fig. 4*C*). A drop in TEER at later time points is inherent to these differentiated primary culture systems since these cells undergo a natural ~5-day lifespan after leaving the stem/progenitor cell state. Interestingly, this may be an intrinsically programmed lifespan as mouse and human epithelial cells in vivo exhibit a similar lifespan (64). Given these features of the culture system, toxin experiments were initiated on *day 3* of differentiation at time $t = 0$ (Fig. 5*A*) as this was between 2 time points that closely mimic the in vivo maturation state, exhibits a relatively high barrier function as measured by TEER, and provides a sufficient window to perform toxicity assays before the cells' terminal lifespan.

To evaluate the sensitivity of the system to detect a range of toxin concentrations, three doses of TcdA were applied apically to mature hCE monolayers. A dose of 30 pM was used as 1× as this is a physiological concentration identified in patients with active CDI (50). TcdA at doses of 30 pM (1×), 150 pM (5×), and 300 pM (10×) was applied to differentiated hCE, and TEER changes were monitored during the first 12 h and after 24 h based on prior evidence of cytotoxicity within that timeframe (Fig. 5*B*) (25, 65). TcdA demonstrated a dose-dependent toxicity whereby 5× and 10× increasingly hastened the onset of barrier loss as measured by TEER. These findings indicate that the hCE culture system is sufficiently sensitive to detect the impact of a clinically relevant range of TcdA concentrations.

An EGFP-ZO-1 Reporter in hCE Monolayers Shows TcdA Exposure Disrupts ZO-1 Localization That Correlates with Loss of Barrier Function

It has been previously demonstrated in the human T84 colon cancer cell line that high doses of TcdA and TcdB disrupt epithelial barrier function by altering membrane localization of tight junction proteins including ZO-1, ZO-2, and occludin (66). To evaluate whether the apical TcdA-dependent drop in TEER correlated with changes in tight junction protein distribution and localization, a fluorescent reporter for tight junction protein localization was genetically engineered into human ISCs. An EGFP-ZO-1 fusion reporter gene was stably integrated by electroporation using a PiggyBac transposon vector system (Fig. 5*C*) (37, 52). The reporter gene was validated by demonstrating that EGFP-tagged ZO-1 proteins colocalized with anti-ZO-1 immunofluorescence staining that evenly distributed to the cell membranes (Fig. 5*D*).

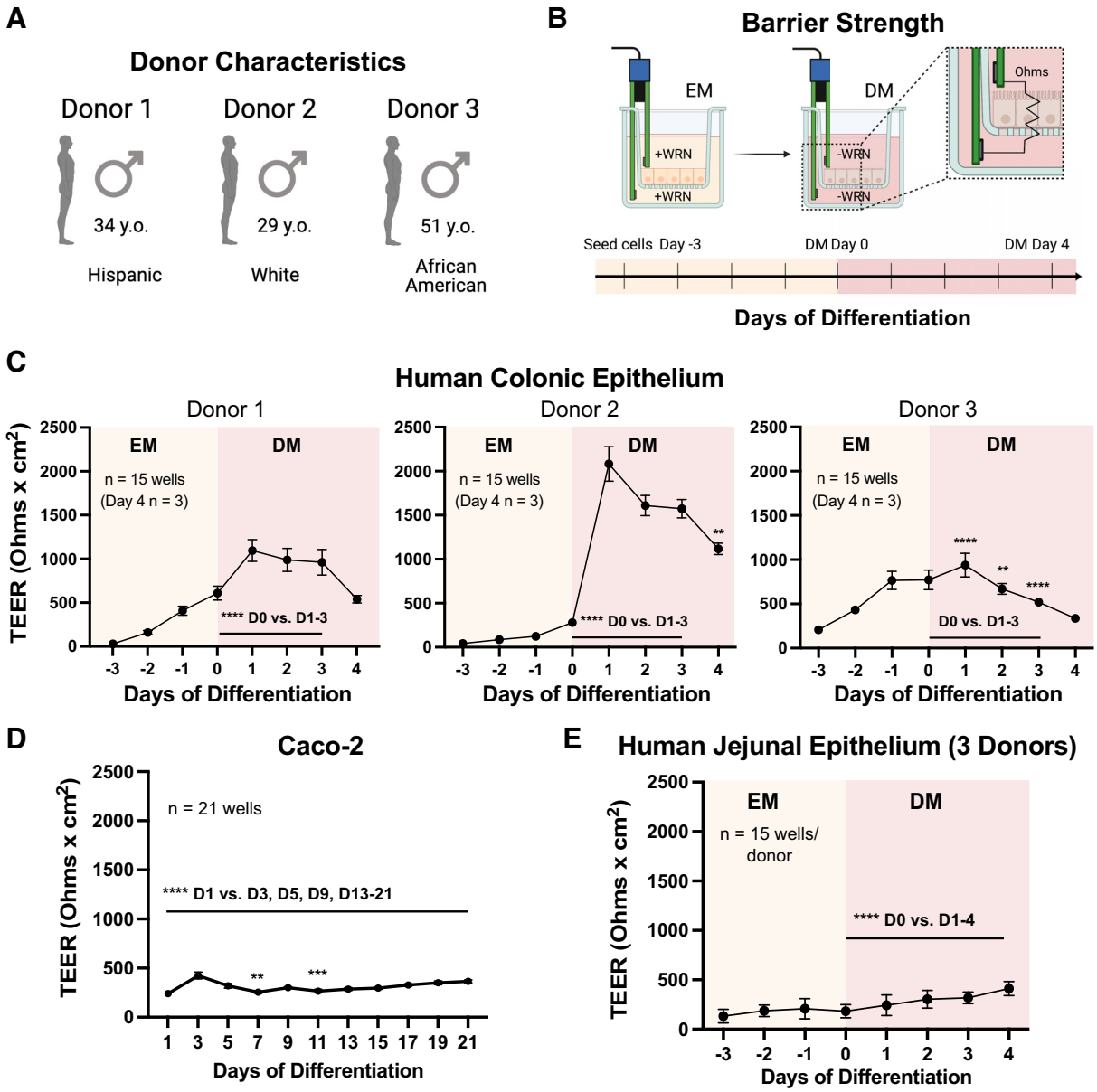

Figure 4. Human colonic epithelial cells exhibit elevated transepithelial electrical resistance (TEER) during differentiation compared with Caco-2 or small intestinal epithelial monolayers. *A*: healthy human organ donor demographic information for TEER assays. *B*: schematic and timeline for TEER (i.e., ionic conductance) measurements during differentiation of human intestinal epithelial monolayers. Monolayer TEER measurements for (*C*) human colonic epithelium, achieving a tight epithelial barrier within 1-day differentiation media (DM) exposure ($N = 3$ donors, $n = 15$ Transwells/donor for all days except $n = 3$ Transwells/donor for *day 4* DM), (*D*) Caco-2 cells ($n = 21$ Transwells), and (*E*) human small intestinal epithelium ($N = 3$ donors, $n = 15$ Transwells/donor). TEER values were compared against TEER at DM D0 (or Caco-2 *day 1*) using a one-way repeated-measures ANOVA with Bonferroni correction. Each data point represents the means ± SD. $^*P < 0.05$, $^{**}P < 0.01$, $^{***}P < 0.001$, $^{****}P < 0.0001$.

To evaluate whether the EGFP-ZO-1 distribution and localization was disrupted following toxin exposure, TcdA was added to the apical surface of the EGFP-ZO-1 hCE monolayers (Fig. 5*E*). Confocal imaging demonstrates aberrant ZO-1 localization after 4 and 8 h of apical TcdA exposure as evidenced by lack of contiguous alignment of ZO-1 with the plasma membrane and accumulation of disjointed ZO-1 puncta (Fig. 5*E*). Importantly, these phenotypic changes correlated with significant drops in TEER at 4 and 8 h of the same concentration and time of TcdA exposure (Fig. 5*B*). These findings highlight the utility of the EGFP-ZO-1 reporter as a rapid and real-time visual readout of *C. difficile* toxicity and establish TEER as a proxy for tight junction integrity in our system.

Transcriptomics Reveals TcdA Induces Expression of Tight Junction and Death Receptor Genes in hCE Monolayers

Transcriptomic changes in hCE caused by *C. difficile* toxins are not known. Evaluating gene expression changes at early stages of toxin exposure could reveal physiological mechanisms of cell injury and targetable mechanisms for therapeutic interventions. Bulk RNAseq was performed on triplicate samples of differentiated hCE treated apically

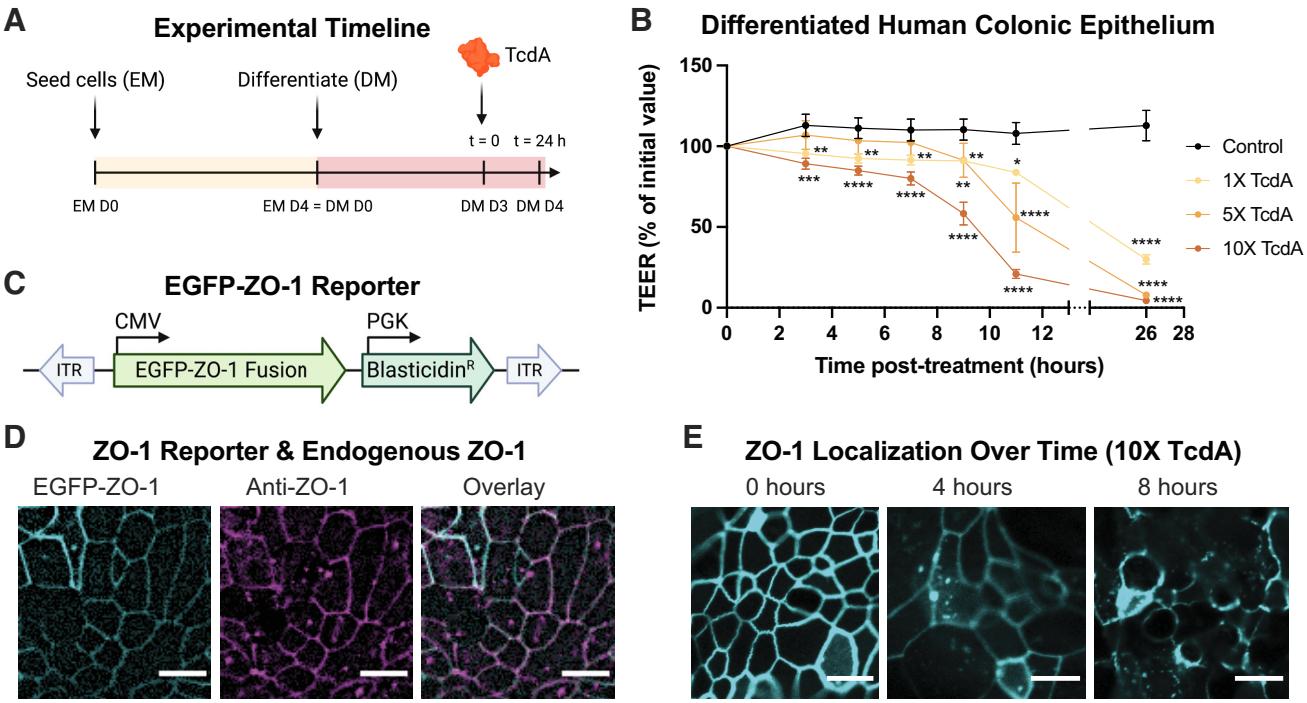

Figure 5. Apical TcdA disrupts ZO-1 localization in EGFP-ZO-1 human colonic epithelium reporter line. *A*: after seeding cells on Transwells in expansion media (EM) and switching to differentiation media (DM), TcdA was added on DM *day 3* (*D3*) at $t = 0$ for 24 h. *B*: dose-response of differentiated human colonic epithelium (hCE) to apical TcdA at 30 pM (1×), 150 pM (5×), or 300 pM (10×); $n = 4$ Transwells, means ± SD. TEER is reported as % of initial value (at $t = 0$). One-way ANOVA followed by Dunnett's multiple comparisons test were used. $^{*}P < 0.05$, $^{**}P < 0.01$, $^{***}P < 0.001$, $^{****}P < 0.0001$. *C*: schematic of EGFP-ZO-1 fusion reporter with a constitutively expressed blasticidin resistance gene. *D*: EGFP-ZO-1 reporter (*left*) in primary human colonic epithelial monolayer, anti-ZO-1 staining (center), and overlay showing colocalization (*right*). Images were taken using a Keyence BZ-X800 fluorescent microscope ×40 objective. *E*: EGFP-ZO-1 reporter line representative images at 0 h (*left*), 4 h (*center*), and 8 h (*right*) after apical exposure to 10× TcdA. Images were taken using a Zeiss LSM710 confocal ×10 objective and ZEN 2011 acquisition software. All scale bars = 10 μm. ITR, inverted terminal repeat; TEER, transepithelial electrical resistance.

with 1× (30 pM) TcdA for 8 and 20 h (Supplemental Fig. S1; https://doi.org/10.6084/m9.figshare.21981050 and Fig. 6). Analyses were focused on tight junction genes and cytokine/cytokine receptor expression at the toxicity "onset phase" (8 h) and "advanced phase" (20 h), which is defined as near-complete loss of TEER (Fig. 5*B*). Tight junction genes were curated using the same panel of 15 differentially expressed genes in mature absorptive cells as in the single-cell RNAseq data (Fig. 2). Interestingly, although most tight junction genes did not show any change in expression after 8 h of TcdA exposure, there was a significant decrease in expression of *TJP1* (*ZO-1*) (Supplemental Fig. S1*A*: https://doi.org/10.6084/m9.figshare.21981050; Supplemental Table S1: https://doi.org/10.6084/m9.figshare.21981056). By contrast, after 20 h of TcdA exposure, 8 out of the 14 tight junction genes that passed the minimum threshold of gene expression were significantly increased (Fig. 6*A* and Supplemental Table S2: https://doi.org/10.6084/m9.figshare.21981047). These data suggest that although *TJP1* expression decreases after early stages of toxin exposure, expression of multiple tight junction genes increases after prolonged TcdA exposure, potentially as a protective response in attempt to re-establish barrier function.

Epithelial cytokine signaling is stimulated by pathogens like *C. difficile* to mount a protective inflammatory response (67). To explore how hCE monolayers might signal through inflammatory cytokines/chemokines and intrinsic receptors, we interrogated gene expression changes after apical 1× TcdA exposure for 8 and 20 h. A curated gene set was assembled based on search terms for epithelial-immune responses including chemokines (CXCL), cytokines (interleukins, IL; interferon, IFN; tumor necrosis factor, TNF) and their receptors/ligands (Supplemental Table S1: https://doi.org/10.6084/m9.figshare.21981056 and Supplemental Table S2: https://doi.org/10.6084/m9.figshare.21981047). During the onset phase of toxicity (8 h post-TcdA), cytokine/chemokine genes were mostly unchanged with only 2 of 46 genes exhibiting downregulation (Supplemental Fig. S1*B*: https://doi.org/10.6084/m9.figshare.21981050). By contrast, at the advanced phase of toxicity (20 h post-TcdA) more cytokine/chemokine genes were changed with 11 genes being downregulated and 7 upregulated (Fig. 6*B*). These data show time-dependent regulation of subsets of cytokines, with downregulation of many chemokines (*CXCL1, CXCL3, CXCL5,* and *CXCL8*) that serve as chemoattractants for immune cell recruitment, and upregulation of TNF receptor superfamily (TNFRSF) genes (*TNFRSF1A, TNFRSF10B, TNFRSF21,* and *TNFRSF25*) known as death receptors.

Basal Exposure to *C. difficile* Toxins A/B Produces More Rapid and Severe Cytotoxicity than Apical Toxin Exposure

An important feature of our platform is the ability to probe the impact of stimuli on the apical versus basal aspect of primary human hCE, which is not easily accessible in 3 D organoid or tissue explant models. To evaluate differential

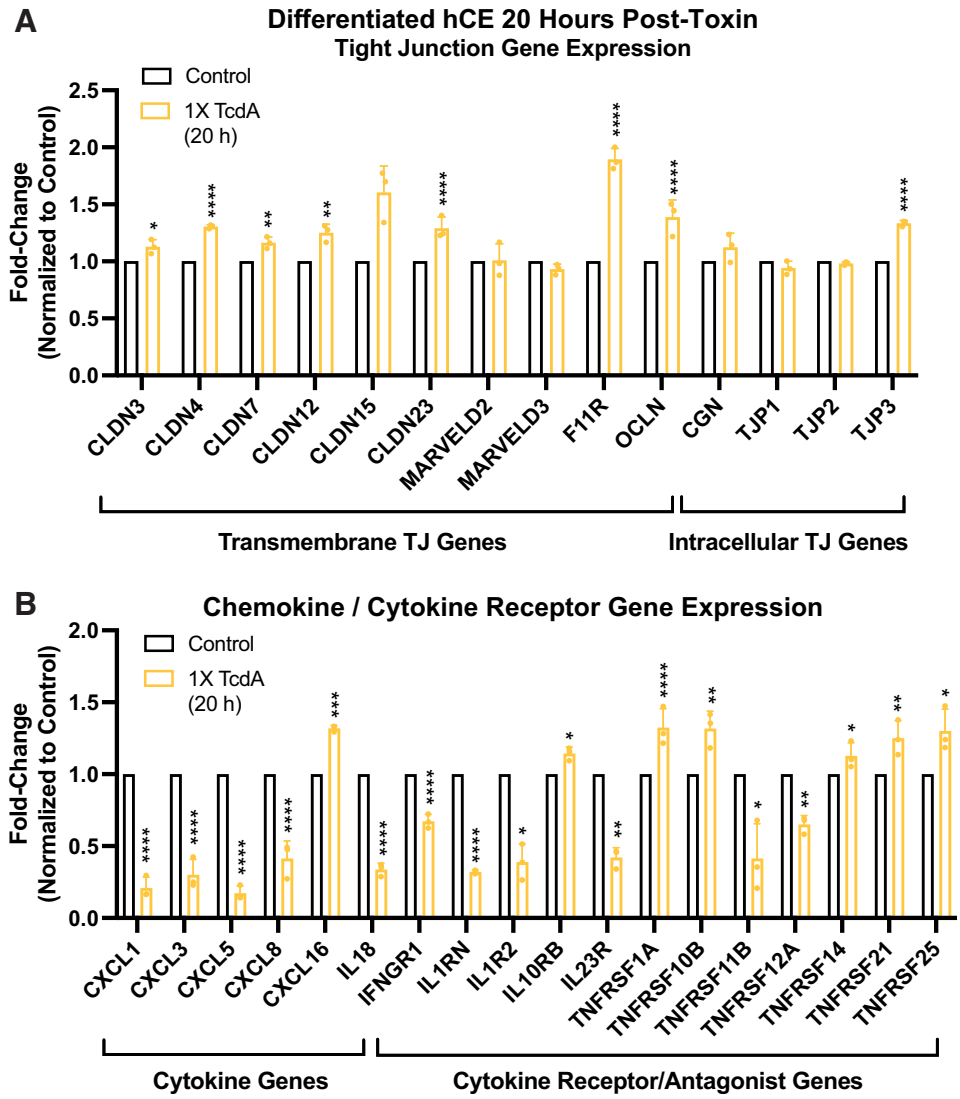

Figure 6. Apical TcdA induces expression of tight junction and death receptor genes in differentiated human colonic epithelium. Bulk RNAseq data showing fold-change of (*A*) transmembrane and intracellular tight junction (TJ) genes and (*B*) cytokine/cytokine receptor genes in differentiated human colonic epithelium (hCE) treated for 20 h apically with 1× TcdA relative to untreated controls; $n = 3$ Transwells, means ± SD. *$q < 0.05$, **$q < 0.01$, ***$q < 0.001$, ****$q < 0.0001$.

sensitivities of apical and basal *C. difficile* toxin at a molar-to-molar ratio, 1× (30 pM) toxin was applied to either the apical or basal reservoirs of Transwells with differentiated hCE or hSIE monolayers from three separate human donors (Fig. 7, *A* and *B*). TcdB applied to the apical aspect of differentiated hCE monolayers from three different donors demonstrated limited and delayed toxicity at 12 h post-TcdB exposure (Fig. 7*A*). By contrast, there was rapid and substantial cytotoxicity as early as 2 h (on average, ~4.7 h) when TcdB was applied to the basal aspect of the monolayers across all donors.

Similarly, there was a trend of significantly delayed toxicity for TcdA when applied to the apical aspect of the monolayers compared with when TcdA was applied to the basal aspect of cells. For 2 donors, the monolayers demonstrated limited apical TcdA cytotoxicity at 12 h, whereas basal exposure to TcdA resulted in rapid onset of cytotoxicity as early as 2 h (on average, 4 h) postexposure across all three donors (Fig. 7*A*). Interestingly, *donor 2* monolayers were more sensitive to apical application of both TcdA/B, and *donor 3* monolayers demonstrated delayed onset of cytotoxicity for both TcdA/B compared with the other two donor monolayers. Overall, TcdA/B demonstrated more cytotoxicity when exposed to the basal aspect of cells. Consistent with this, hCE monolayers were refractory to apoptosis at 24 h after apical TcdA or TcdB exposure, whereas basal toxin exposure caused obvious signs of apoptosis (Fig. 7*C*). Differential toxin sensitivities observed between donors is interesting and may reflect genetic backgrounds that render the differentiated hCE monolayers more or less responsive to the mechanisms of toxicity, which could be useful for determining patient-specific responses.

Single-cell RNAseq data of the *C. difficile* receptor gene expression profiles demonstrated that 2 of 3 known TcdA receptor genes (*SI* and *LRP1*) have significantly higher gene expression in mature absorptive lineages of the small intestine versus colon (Fig. 2*B*). Thus, we hypothesized that differentiated hSIE monolayers would be more sensitive than differentiated hCE monolayers to TcdA. When TcdA was applied to the apical aspect of monolayers, substantial cytotoxicity was observed in hSIE monolayers as early as 2 h (on average, 4 h; Fig. 7*B*). By comparison, differentiated hCE demonstrated limited apical TcdA cytotoxicity in 2 donors with a late onset of 12–24 h (on average, 12 h across all

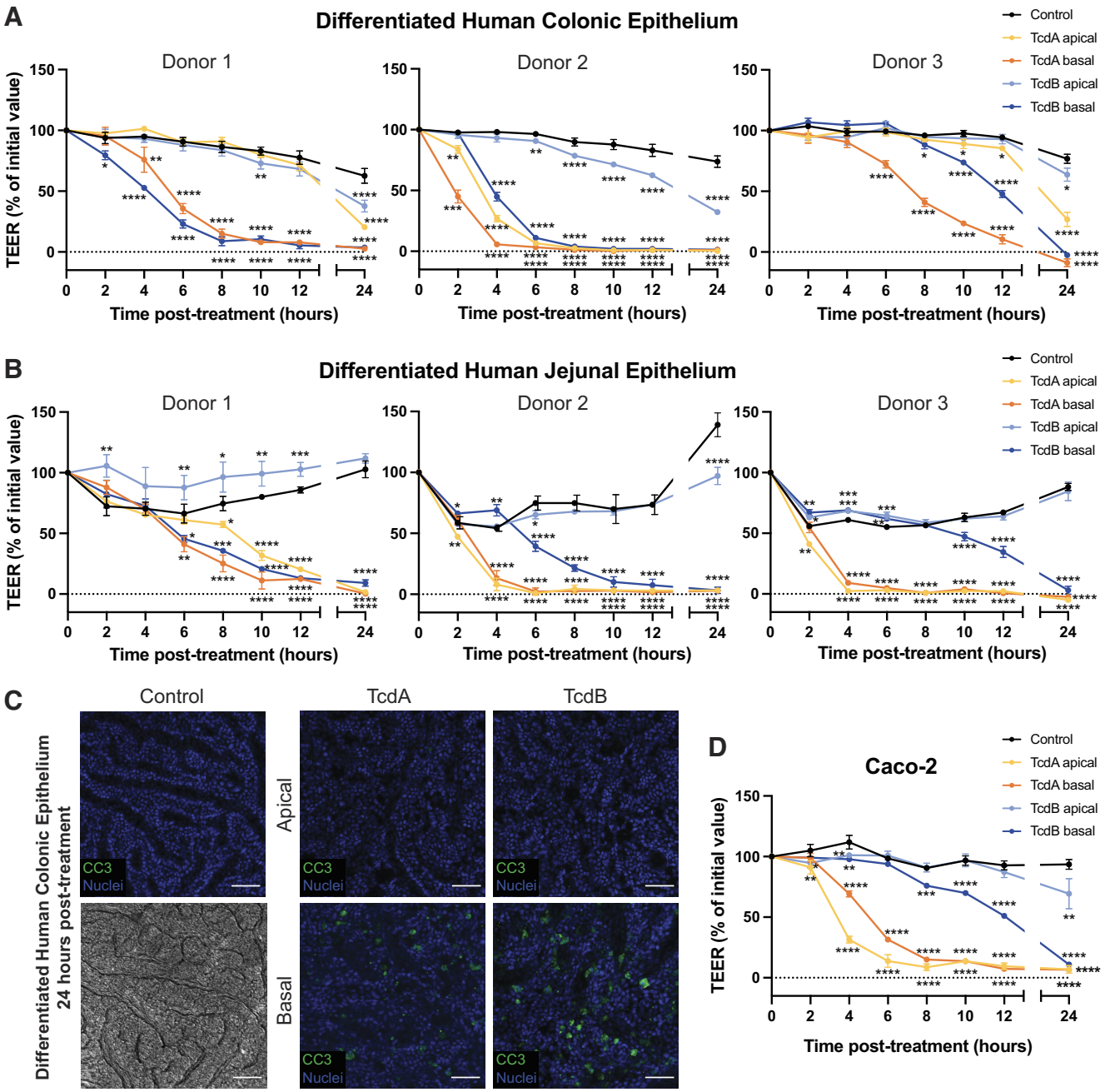

Figure 7. Basal *Clostridioides difficile* TcdA/B exposure induces more rapid cytotoxicity than apical toxin exposure in differentiated human colonic epithelium. Monolayer TEER measurements for differentiated (*A*) human colonic epithelium (hCE) and (*B*) human jejunal epithelium. *C*: representative immunofluorescence staining (CC3, cleaved-caspase 3; Nuclei, bisbenzimide) and brightfield image (Control) of fixed apical/basal TcdA or TcdB-treated hCE, 24 h post-treatment. Images were taken using a Zeiss LSM710 confocal 10× objective and ZEN 2011 acquisition software, with postacquisition processing using FIJI. All scalebars = 50 μm. *D*: TEER measurements for differentiated Caco-2 monolayers after apical or basal addition of TcdA or TcdB. Toxins were added to DM at 1× = 30 pM; $n = 3$ donors for human colon and jejunum, and $n = 3$ Transwells, means ± SD. One-way ANOVA followed by Dunnett's multiple comparisons test were used. $^{*}P < 0.05$, $^{**}P < 0.01$, $^{***}P < 0.001$, $^{****}P < 0.0001$.

donors; Fig. 7*A*). These findings show that differentiated hSIE is more sensitive to apical exposure to TcdA compared with differentiated hCE. Of note, TcdA/B cytotoxicity in Caco-2 monolayers is more consistent with trends observed in the hSIE monolayers compared with the hCE monolayers, with rapid sensitivity to apical TcdA within 2–4 h and a relatively slower response to basal TcdB (Fig. 7*D*). This highlights that, despite being derived from colon epithelial cancer, Caco-2 cells respond to toxins more like hSIE than hCE monolayers.

A Leaky hCE Induced by NSAIDs Reduces Apical Barrier Protection from TcdB

Our results so far suggest limited sensitivity to TcdB on the apical/luminal surface of the human colon, but enhanced TcdB toxicity when applied to the basal surface. We hypothesized

that toxin translocation from the apical to the basal side may be initiated or enhanced by a "leaky gut," a term used to describe a broad range of underlying genetic, disease, or injury states that create increased intestinal paracellular permeability (68). NSAIDs in general are associated with colitis (69), and diclofenac (DCF) in particular has demonstrated a significantly increased risk of *C. difficile*-associated diarrhea (70, 71). Diclofenac, a commonly prescribed NSAID, has been previously shown to induce a leaky gut in primary hSIE (72). Clinically relevant dosing of 1 mM was determined based on translating a typical therapeutic dose of 50 mg oral diclofenac into local concentrations of diclofenac between 300 and 1,600 μM within the intestinal lumen (73–75).

Although TEER is an effective method to monitor ion flux across a damaged epithelial monolayer, it may not accurately report flux of toxin-sized molecules. To test whether a leaky gut induced by diclofenac initiates apical-to-basal translocation of toxin-sized molecules, a permeability assay was designed using hCE monolayers to monitor the translocation of conjugated dextrans from the apical to basal reservoir after toxin exposure (Fig. 8). Large-molecular-weight dextrans should remain in the apical reservoir of the Transwells if there is a healthy epithelial barrier. FITC-Dextran (250 kDa) was chosen because it is similar to the molecular weight of TcdB (~270 kDa), which would provide insight into the time course in which a TcdB-sized particle would be able to pass paracellularly when the epithelial barrier is damaged. In the first 12 h, apical diclofenac exposure alone induced modest leakiness which was compounded by the apical addition of TcdB, as measured by FITC-Dextran permeability (Fig. 8). Of all the TcdB experimental conditions, increased permeability was only observed in the diclofenac/TcdB condition at 12 h, consistent with the idea that epithelial barrier damage was allowing TcdB to interact with the basal aspect of the monolayer. At 24 h, apical diclofenac/TcdB continued to show significantly increased permeability of FITC-Dextran, trending toward permeability levels that are only induced by direct application of TcdB to the basal side of the hCE monolayer (Fig. 8). Taken together, these findings further reveal that a leaky colonic epithelial barrier can enhance the cytotoxic effects of apical TcdB exposure, likely through a mechanism whereby TcdB gains access to the basal aspect of the epithelial monolayer.

DISCUSSION

In this work, we describe uncoupled apical and basal toxicity of *C. difficile* TcdA/B on hCE in multiple healthy human donors. We demonstrate that toxin sensitivities differ between hCE and hSIE, which could be related to different magnitudes of toxin receptor distribution across anatomical regions of the gut as revealed by our transcriptomic data. This interpretation is supported by findings that some toxin receptors are preferentially located on the apical versus basal surface of small intestinal or colonic epithelium (28–33, 54). The importance of identifying uncoupled apical/basal magnitude and time course of TcdA/B cytotoxicities is that these findings may help inform the approach to develop more effective therapeutic modalities. As basal toxin exposure has more substantial cytotoxic effects, the use of luminal therapeutics such as probiotics or toxin-neutralizing drugs could be used as prophylaxis to prevent toxins from reaching the basal surface where they have more potent effects. This also has important clinical implications for patients with underlying intestinal epithelial barrier dysfunction, suggesting that they may have greater sensitivity to *C. difficile* toxins due to basal receptor interactions.

Although 3 D organoids and 2 D monolayers are becoming more widely used to study host-microbe interactions, here we specifically tailor and characterize a first-in-kind 2 D monolayer system in vitro that closely mimics the transcriptomic state of late ACCs found in vivo. We then focus the assay development in the system to detect the first signs of barrier loss caused by *C. difficile* toxins. Although preclinical intestinal models traditionally focus on genetically homogenous Caco-2 cells and other cell lines (16–19, 76–79), our transcriptomic data and barrier strength readouts show that Caco-2 cells remain in a relatively undifferentiated state and have a more similar barrier function profile to hSIE monolayers. This suggests that the hCE monolayers developed in our system are likely a more accurate preclinical model to evaluate toxin effects that are observed in the primary anatomical location in patients affected by CDI (27).

The use of cancer cell lines such as Caco-2 as models to investigate biological mechanisms or preclinical models for drug testing comes with some advantages, such as ease/low cost of use and reproducible readouts. On the other hand, they suffer from homogenous responses that likely will not

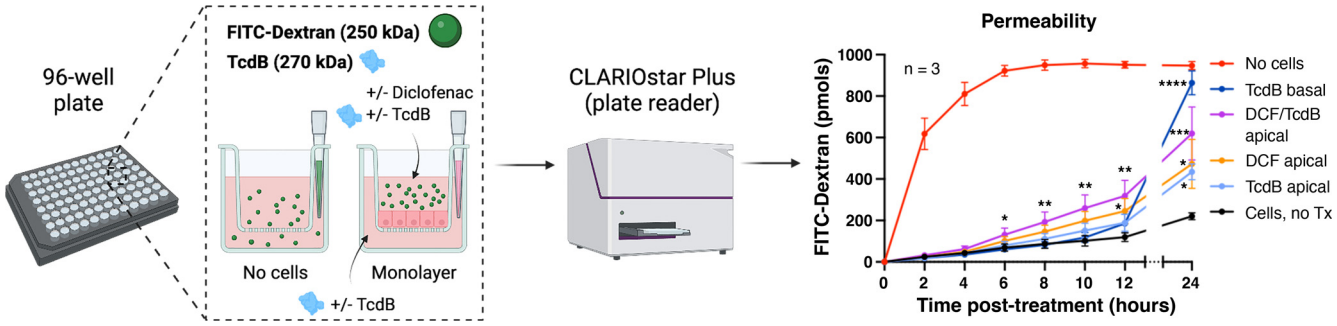

Figure 8. A leaky human colonic epithelium induced by diclofenac reduces apical barrier protection from TcdB. Schematic showing TcdB-sized FITC-Dextran (250 kDa) added to the apical surface of Transwells with or without differentiated human colonic epithelium (hCE), +/− TcdB, and +/− diclofenac and resulting permeability ($n = 3$ Transwells). Permeability data show cumulative FITC-Dextran (pmol) transported from apical to basal compartments of Transwells. Each data point represents the means ± SD. One-way ANOVA followed by Dunnett's multiple comparisons test were used. *$P < 0.05$, **$P < 0.01$, ***$P < 0.001$, ****$P < 0.0001$. Tx, treatment.

report the variability of responses observed in the human population. We view the inherent variability observed between hCE monolayers derived from different donors as an advantage as it has the potential to capture variability that exists in the human population. In this study, healthy transplant-grade tissue from three adult male donors varying in age and race/ethnicity was used. However, the ease of the hCE toxicity assay renders it scalable to additional donor demographics for increased representation of variable responses between humans. For example, *donor 2* appeared to be unusually sensitive to apically applied TcdA. Although we cannot attribute a cause, unlike the other two donors, *donor 2* is White, and there is evidence to suggest that White patients demonstrate a higher CDI rate than patients of other races or ethnicities (80). Although we acknowledge that sample sizes would have to be increased to confirm a statistical association, this example shows that our system allows sufficiently sensitive detection of toxin responses between humans. Ongoing efforts to bank ISCs from female and pediatric donors will allow us to evaluate the role of sex and age on *C. difficile* toxicity. Notably, this could increase the predictive value of our system as a preclinical model and address a substantial limitation of the genetically homogenous Caco-2 cell line.

Another major strength of this model is that it allows us to consider *C. difficile* toxin effects as a multistep process: early barrier dysfunction (onset of TEER drop) that leads to increased paracellular permeability (FITC-Dextran basal accumulation), cell rounding, and then eventual cytotoxic cell death (apoptosis) (Fig. 9). Whereas currently used cell culture cytotoxicity assays that characterize cell rounding come with subjective readouts are nonstandardized and require 24–48 h of incubation (81), our platform sensitively and quantitatively captures effects of TcdA/B in as little as 2 h. Notably, although this platform was designed to evaluate the earliest events in toxicity on differentiated epithelium, the transcriptomic data collected from cells in EM suggest that this platform could also be used to evaluate the impact of toxins on the stem/undifferentiated cell lineages, which to-date has not been fully characterized but has clinically relevant implications for wound healing and epithelial regeneration in CDI (82).

An additional example of how transcriptomics can be paired with this model is to evaluate the impact of toxins on expression of genes such as cytokines and their receptors. Epithelial cells can release cytokines/chemokines in response to cellular stress, so the downregulation of cytokines at the advanced phase of toxicity was not intuitive but suggests that mechanisms are in place to moderate immune cell infiltration mediated by many of the cytokines. IL-8 in particular (encoded by *CXCL8*) demonstrated downregulation at both onset and advanced phases of toxicity. This was intriguing as studies using immortalized cell lines and biopsy samples exposed to TcdA show increased IL-8 expression (83–85). We explored the experimental design of these studies and found that TcdA concentrations were up to 750,000 times higher than the physiological TcdA concentrations used in this study (30 pM) (50). There is evidence that IL-8 upregulation is absent at TcdA doses $\leq$ 10 ng/mL, a dose consistent with our 1× TcdA condition (30 pM, ~9.2 ng/mL) (86); therefore, a plausible interpretation is that healthy hCE monolayers may be more refractory to TcdA-mediated upregulation of cytokines at physiologically relevant TcdA concentrations than previously suggested by other human colon models, though further study is warranted.

Notably, during advanced stages of toxicity, gene expression of 4 cytokine receptors in the TNFRSF subgroup known as death receptors was significantly upregulated in response to apical 1× TcdA exposure. These receptors are known to play an important role in apoptosis induction through their respective ligands including TNF-α, TRAIL (TNFSF10), and TL1A (TNFSF15) (87). Interestingly, most of the TNFRSF ligands were below the limit of minimum gene expression or not significantly changed relative to controls, suggesting that stimulation of the death receptors primarily comes from extrinsic ligands rather than an autocrine loop (Supplemental Table S2: https://doi.org/10.6084/m9.figshare.21981047).

Upregulation of TNF receptors is novel and clinically relevant given that the antibiotic fidaxomicin, associated with reduced recurrence of CDI, has been shown to inhibit TcdA-induced TNF-α mRNA expression in human colonic explants (88). Although prior studies in ovarian and colon carcinoma cell lines demonstrated a death receptor-independent mechanism of TcdA-induced apoptosis (89), this mechanism has not been investigated in primary hCE. This further highlights the role of TNF receptor signaling in response to *C. difficile* toxins and introduces death receptors as potential targets for future

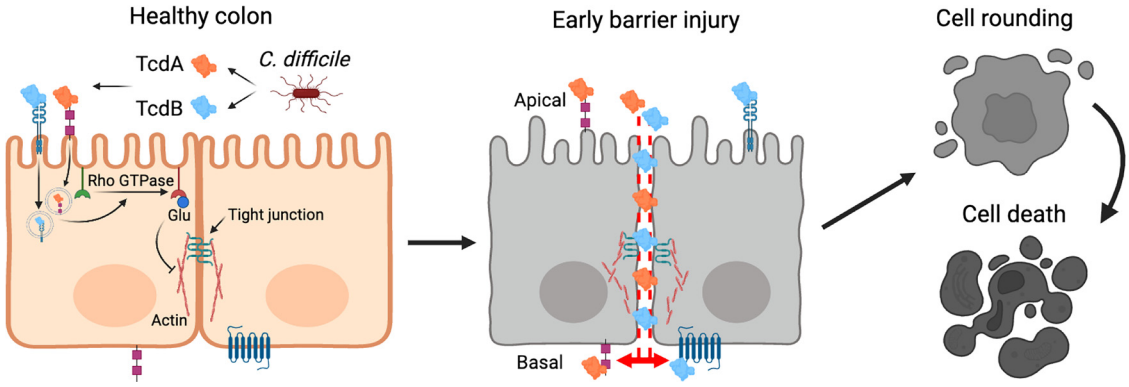

Figure 9. Human colonic epithelial cell platform detects early evidence of *Clostridioides difficile* toxicity. TcdA and TcdB enzymatic toxins are secreted by *C. difficile*, bind to host receptors, enter cells via endocytosis, and inactivate Rho-family GTPases by monoglucosylation. This results in early barrier injury, increased paracellular permeability to toxins, cell rounding, and eventual apoptosis.

investigation in mediating the hCE-immune response to CDI. Overall, this platform represents a flexible system and a strong experimental foundation to evaluate mechanisms of cell death or other aspects of cellular toxicities for development of new therapeutic approaches.

Beyond studying *C. difficile* toxicity, the hCE platform and EGFP-ZO-1 hCE reporter established here can be utilized for a wide range of translational research applications, such as evaluating the toxicity of other pathogens, modeling a leaky/inflamed hCE, and drug screening. The fluorescent ZO-1 reporter can be used to live image tight junctions during epithelial barrier disruption, showing promise for future studies on mechanisms of injury progression or therapeutic efficacy to restore barrier function. Although we tailored the hCE monolayers in this study to detect and monitor the impacts of *C. difficile* toxins A/B, our methodological approach could be applied to other host-microbe interactions. For example, *Vibrio cholerae* and toxigenic *Escherichia coli*, which both are associated with life-threatening diarrhea, produce toxins that impact other colonic physiological properties such as water and ion transport that could be further characterized using the transcriptomic and experimental tools highlighted in this study (90, 91). In addition, given that intestinal barrier defects are associated with a variety of human pathologies and diseases, the leaky gut model could be expanded to study other disease states associated with intestinal barrier defects including IBD, celiac disease, and irritable bowel syndrome (68) to understand how these underlying conditions could potentiate disease etiology and negative effects of pathogenic microbes.

DATA AVAILABILITY

Data will be made available upon reasonable request.

SUPPLEMENTAL DATA

Supplemental Fig. S1: https://doi.org/10.6084/m9.figshare.21981050.

Supplemental Table S1: https://doi.org/10.6084/m9.figshare.21981056.

Supplemental Table S2: https://doi.org/10.6084/m9.figshare.21981047.

ACKNOWLEDGMENTS

First and foremost, the authors thank the anonymous organ donors, their families, and HonorBridge (Durham, NC) for providing the intestinal tissue samples used in this study. Schematics in Figs. 1*A*, 3*A*, 4*A*, 4*B*, 5*A*, 5*C*, 8, and 9 were created using BioRender. The authors also thank the UNC High-Throughput Sequencing Facility and the CGIBD Advanced Analytics Core, especially Gabrielle Cannon, for RNAseq data. The authors thank Alan Fanning for the pEGFP ZO-1 plasmid; Casey Theriot, Rita Tamayo, Carly Catella, Carol Hall, Sudeep Sarma, Nick Markham, and Aadra Bhatt for useful discussions; and James Stroud, Nathan Kohn, and Yunan Hu for support with TEER measurements.

GRANTS

This study was supported by National Institute of Diabetes and Digestive and Kidney Diseases (NIDDK) Grants R01DK115806 (to S.T.M.), R01DK109559 (to S.T.M.), P30DK034987 (to S.T.M.), R43DK12515 (to S.T.M.); National Science Foundation Grant CBET-1934284 (to S.T.M.); the Katherine E. Bullard Charitable Trust for Gastrointestinal Stem Cell and Regenerative Research (to S.T.M.); and NIDDK Grants F30DK126307 (to M.T.O), F32DK124929 (to J.B.), T32GM133364 (to K.A.B).

DISCLOSURES

S.T.M. has a financial interest in Altis Biosystems Inc., which licenses the technology used in this study. None of the other authors has any conflicts of interest, financial or otherwise, to disclose.

AUTHOR CONTRIBUTIONS

M.T.O., J.L., and S.T.M. conceived and designed research; M.T.O., J.L., C.M.H., and E.E.T.S.P. performed experiments; M.T.O., J.L., R.J.B., C.M.H., E.E.T.S.P., K.A.B., I.G.-M., and J.B. analyzed data; M.T.O., R.J.B., C.M.H., K.A.B., I.G.-M., J.B., and S.T.M. interpreted results of experiments; M.T.O. and J.L. prepared figures; M.T.O. and J.L. drafted manuscript; M.T.O., J.L., R.J.B., C.M.H., K.A.B., I.G.-M., J.B., and S.T.M. edited and revised manuscript; M.T.O., J.L., R.J.B., C.M.H., E.E.T.S.P., K.A.B., I.G.-M., J.B., and S.T.M. approved final version of manuscript.

REFERENCES

1. **Kordus SL**, **Thomas AK**, **Lacy DB.** *Clostridioides difficile* toxins: mechanisms of action and antitoxin therapeutics. *Nat Rev Microbiol* 20: 285–298, 2021. doi:10.1038/s41579-021-00660-2.
2. **Zhang S**, **Palazuelos-Munoz S**, **Balsells EM**, **Nair H**, **Chit A**, **Kyaw MH.** Cost of hospital management of *Clostridium difficile* infection in United States—a meta-analysis and modelling study. *BMC Infect Dis* 16: 447, 2016. doi:10.1186/s12879-016-1786-6.
3. **Nitzan O.** Clostridium difficile and inflammatory bowel disease: role in pathogenesis and implications in treatment. *World J Gastroenterol* 19: 7577–7785, 2013. doi:10.3748/wjg.v19.i43.7577.
4. **Johnson S**, **Lavergne V**, **Skinner AM**, **Gonzales-Luna AJ**, **Garey KW**, **Kelly CP**, **Wilcox MH.** Clinical Practice Guideline by the Infectious Diseases Society of America (IDSA) and Society for Healthcare Epidemiology of America (SHEA): 2021 Focused Update Guidelines on Management of *Clostridioides difficile* infection in adults. *Clin Infect Dis* 73: e1029–e1044, 2021. doi:10.1093/cid/ciab549.
5. **Peng Z**, **Jin D**, **Kim HB**, **Stratton CW**, **Wu B**, **Tang Y-W**, **Sun X.** Update on antimicrobial resistance in clostridium difficile: resistance mechanisms and antimicrobial susceptibility testing. *J Clin Microbiol* 55: 1998–2008, 2017. doi:10.1128/JCM.02250-16.
6. **Kelly CP**, **Lamont JT.** *Clostridium difficile*— more difficult than ever. *N Engl J Med* 359: 1932–1940, 2008 [Erratum in *N Engl J Med* 363: 1585, 2010]. doi:10.1056/NEJMra0707500.
7. **Louie TJ**, **Miller MA**, **Mullane KM**, **Weiss K**, **Lentnek A**, **Golan Y**, **Gorbach S**, **Sears P**, **Shue Y-K**; **OPT-80-003 Clinical Study Group.** Fidaxomicin versus vancomycin for *Clostridium difficile* infection. *N Engl J Med* 364: 422–431, 2011. doi:10.1056/NEJMoa0910812.
8. **Kuehne SA**, **Collery MM**, **Kelly ML**, **Cartman ST**, **Cockayne A**, **Minton NP.** Importance of toxin A, toxin B, and CDT in virulence of an epidemic *Clostridium difficile* strain. *J Infect Dis* 209: 83–86, 2014. doi:10.1093/infdis/jit426.
9. **Martinez-Melendez A**, **Cruz-Lopez F**, **Morfin-Otero R**, **Maldonado-Garza HJ**, **Garza-Gonzalez E.** An update on *Clostridioides difficile* binary toxin. *Toxins (Basel)* 14: 305, 2022. doi:10.3390/toxins14050305.
10. **Voth DE**, **Ballard JD.** *Clostridium difficile* toxins: mechanism of action and role in disease. *Clin Microbiol Rev* 18: 247–263, 2005. doi:10.1128/CMR.18.2.247-263.2005.
11. **Orrell KE**, **Melnyk RA.** Large clostridial toxins: mechanisms and roles in disease. *Microbiol Mol Biol Rev* 85: e0006421, 2021. doi:10.1128/MMBR.00064-21.
12. **Orrell KE**, **Zhang Z**, **Sugiman-Marangos SN**, **Melnyk RA.** *Clostridium difficile* toxins A and B: receptors, pores, and translocation into cells. *Crit Rev Biochem Mol Biol* 52: 461–473, 2017. doi:10.1080/10409238.2017.1325831.

13. **Aktories K**, **Schwan C**, **Jank T.** *Clostridium difficile* toxin biology. *Annu Rev Microbiol* 71: 281–307, 2017. doi:10.1146/annurev-micro-090816-093458.
14. **Hecht G**, **Pothoulakis C**, **LaMont JT**, **Madara JL.** *Clostridium difficile* toxin A perturbs cytoskeletal structure and tight junction permeability of cultured human intestinal epithelial monolayers. *J Clin Invest* 82: 1516–1524, 1988. doi:10.1172/JCI113760.
15. **Hecht G**, **Koutsouris A**, **Pothoulakis C**, **LaMont JT**, **Madara JL.** *Clostridium difficile* toxin B disrupts the barrier function of T84 monolayers. *Gastroenterology* 102: 416–423, 1992. doi:10.1016/0016-5085(92)90085-d.
16. **Du T**, **Mj A.** Translocation of *Clostridium difficile* toxin B across polarized caco-2 cell monolayers is enhanced by toxin A. *Can J Inf Dis* 15: 83–88, 2004. doi:10.1155/2004/292580.
17. **Rothman SW**, **Brown JE**, **Diecidue A**, **Foret DA.** Differential cytotoxic effects of toxins A and B isolated from *Clostridium difficile*. *Infect Immun* 46: 324–331, 1984. doi:10.1128/iai.46.2.324-331.1984.
18. **Sutton PA**, **Li S**, **Webb J**, **Solomon K**, **Brazier J**, **Mahida YR.** Essential role of toxin A in *C. difficile* 027 and reference strain supernatant-mediated disruption of Caco-2 intestinal epithelial barrier function. *Clin Exp Immunol* 153: 439–447, 2008. doi:10.1111/j.1365-2249.2008.03690.x.
19. **Carter GP**, **Rood JI**, **Lyras D.** The role of toxin A and toxin B in *Clostridium difficile*-associated disease: past and present perspectives. *Gut Microbes* 1: 58–64, 2010. doi:10.4161/gmic.1.1.10768.
20. **Kleiveland CR.** *Co-cultivation of Caco-2 and HT-29MTX*. Springer International Publishing, 2015, p. 135–140.
21. **Lea T.** Caco-2 cell line. In: *The Impact of Food Bioactives on Health: In Vitro and Ex Vivo Models*, edited by Verhoeckx K, Cotter P, López-Expósito I, Kleiveland C, Lea T, Mackie A, Requena T, Swiatecka D, and Wichers H. Cham, Switzerland: Springer, 2015.
22. **Chaves-Olarte E**, **Weidmann M**, **Eichel-Streiber C**, **Thelestam M.** Toxins A and B from Clostridium difficile differ with respect to enzymatic potencies, cellular substrate specificities, and surface binding to cultured cells. *J Clin Invest* 100: 1734–1741, 1997. doi:10.1172/JCI119698.
23. **Donta ST**, **Sullivan N**, **Td W.** Differential effects of *Clostridium difficile* toxins on tissue-cultured cells. *J Clin Microbiol* 15: 1157–1158, 1982. doi:10.1128/jcm.15.6.1157-1158.1982.
24. **Leslie JL**, **Huang S**, **Opp JS**, **Nagy MS**, **Kobayashi M**, **Young VB**, **Spence JR.** Persistence and toxin production by *Clostridium difficile* within human intestinal organoids result in disruption of epithelial paracellular barrier function. *Infect Immun* 83: 138–145, 2015. doi:10.1128/IAI.02561-14.
25. **Engevik MA**, **Danhof HA**, **Chang-Graham AL**, **Spinler JK**, **Engevik KA**, **Herrmann B**, **Endres BT**, **Garey KW**, **Hyser JM**, **Britton RA**, **Versalovic J.** Human intestinal enteroids as a model of *Clostridioides difficile*-induced enteritis. *Am J Physiol Gastrointest Liver Physiol* 318: G870–G888, 2020. doi:10.1152/ajpgi.00045.2020.
26. **Spence JR**, **Mayhew CN**, **Rankin SA**, **Kuhar MF**, **Vallance JE**, **Tolle K**, **Hoskins EE**, **Kalinichenko VV**, **Wells SI**, **Zorn AM**, **Shroyer NF**, **Wells JM.** Directed differentiation of human pluripotent stem cells into intestinal tissue in vitro. *Nature* 470: 105–109, 2011. doi:10.1038/nature09691.
27. **Fordtran JS.** Colitis due to *Clostridium difficile* toxins: underdiagnosed, highly virulent, and nosocomial. *Proc (Bayl Univ Med Center)* 19: 3–12, 2006. doi:10.1080/08998280.2006.11928114.
28. **Na X**, **Kim H**, **Moyer MP**, **Pothoulakis C**, **Lamont JT.** gp96 is a human colonocyte plasma membrane binding protein for *Clostridium difficile* toxin A. *Infect Immun* 76: 2862–2871, 2008. doi:10.1128/IAI.00326-08.
29. **Schottelndreier D**, **Langejurgen A**, **Lindner R**, **Genth H.** Low density lipoprotein receptor-related protein-1 (LRP1) is involved in the uptake of *Clostridioides difficile* toxin A and serves as an internalizing receptor. *Front Cell Infect Microbiol* 10: 565465, 2020. doi:10.3389/fcimb.2020.565465.
30. **Marzolo M-P**, **Yuseff MI**, **Retamal C**, **Donoso M**, **Ezquer F**, **Farfán P**, **Li Y**, **Bu G.** Differential distribution of low-density lipoprotein-receptor-related protein (LRP) and megalin in polarized epithelial cells is determined by their cytoplasmic domains. *Traffic* 4: 273–288, 2003. doi:10.1034/j.1600-0854.2003.00081.x.
31. **Tao L**, **Zhang J**, **Meraner P**, **Tovaglieri A**, **Wu X**, **Gerhard R**, **Zhang X**, **Stallcup WB**, **Miao J**, **He X**, **Hurdle JG**, **Breault DT**, **Brass AL**, **Dong M.** Frizzled proteins are colonic epithelial receptors for *C. difficile* toxin B. *Nature* 538: 350–355, 2016. doi:10.1038/nature19799.
32. **Chen P**, **Tao L**, **Wang T**, **Zhang J**, **He A**, **Lam K-H**, **Liu Z**, **He X**, **Perry K**, **Dong M**, **Jin R.** Structural basis for recognition of frizzled proteins by *Clostridium difficile* toxin B. *Science* 360: 664–669, 2018. doi:10.1126/science.aar1999.
33. **Vincan E**, **Darcy PK**, **Farrelly CA**, **Faux MC**, **Brabletz T**, **Ramsay RG.** Frizzled-7 dictates three-dimensional organization of colorectal cancer cell carcinoids. *Oncogene* 26: 2340–2352, 2007. doi:10.1038/sj.onc.1210026.
34. **LaFrance ME**, **Farrow MA**, **Chandrasekaran R**, **Sheng J**, **Rubin DH**, **Lacy DB.** Identification of an epithelial cell receptor responsible for *Clostridium difficile* TcdB-induced cytotoxicity. *Proc Natl Acad Sci USA* 112: 7073–7078, 2015. doi:10.1073/pnas.1500791112.
35. **Xie L**, **Fletcher RB**, **Bhatia D**, **Shah D**, **Phipps J**, **Deshmukh S**, **Zhang H**, **Ye J**, **Lee S**, **Le L**, **Newman M**, **Chen H**, **Sura A**, **Gupta S**, **Sanman LE**, **Yang F**, **Meng W**, **Baribault H**, **Vanhove GF**, **Yeh W-C**, **Li Y**, **Lu C.** Robust colonic epithelial regeneration and amelioration of colitis via FZD-specific activation of Wnt signaling. *Cell Mol Gastroenterol Hepatol* 14: 435–464, 2022. doi:10.1016/j.jcmgh.2022.05.003.
36. **Gomez-Martinez I**, **Bliton RJ**, **Breau KA**, **Czerwinski MJ**, **Williamson IA**, **Wen J**, **Rawls JF**, **Magness ST.** A planar culture model of human absorptive enterocytes reveals metformin increases fatty acid oxidation and export. *Cell Mol Gastroenterol Hepatol* 14: 409–434, 2022. doi:10.1016/j.jcmgh.2022.04.009.
37. **Breau KA**, **Ok MT**, **Gomez-Martinez I**, **Burclaff J**, **Kohn NP**, **Magness ST.** Efficient transgenesis and homology-directed gene targeting in monolayers of primary human small intestinal and colonic epithelial stem cells. *Stem Cell Reports* 17: 1493–1506, 2022. doi:10.1016/j.stemcr.2022.04.005.
38. **Wang Y**, **DiSalvo M**, **Gunasekara DB**, **Dutton J**, **Proctor A**, **Lebhar MS**, **Williamson IA**, **Speer J**, **Howard RL**, **Smiddy NM**, **Bultman SJ**, **Sims CE**, **Magness ST**, **Allbritton NL.** Self-renewing monolayer of primary colonic or rectal epithelial cells. *Cell Mol Gastroenterol Hepatol* 4: 165–182.e7, 2017. doi:10.1016/j.jcmgh.2017.02.011.
39. **Burclaff J**, **Bliton RJ**, **Breau KA**, **Ok MT**, **Gomez-Martinez I**, **Ranek JS**, **Bhatt AP**, **Purvis JE**, **Woosley JT**, **Magness ST.** A proximal-to-distal survey of healthy adult human small intestine and colon epithelium by single-cell transcriptomics. *Cell Mol Gastroenterol Hepatol* 13: 1554–1589, 2022. doi:10.1016/j.jcmgh.2022.02.007.
40. **Wolf FA**, **Angerer P**, **Theis FJ.** SCANPY: large-scale single-cell gene expression data analysis. *Genome Biol* 19: 15, 2018. doi:10.1186/s13059-017-1382-0.
41. **Pedregosa F**, **Varoquaux G**, **Michel V**, **Thirion B.** Scikit-learn: machine learning in Python. *J Mach Learn Res* 12: 2825–2830, 2011. https://www.jmlr.org/papers/volume12/pedregosa11a/pedregosa11a.pdf?ref=https:/.
42. **Love MI**, **Huber W**, **Anders S.** Moderated estimation of fold change and dispersion for RNA-seq data with DESeq2. *Genome Biol* 15: 550, 2014. doi:10.1186/s13059-014-0550-8.
43. **Subramanian A**, **Tamayo P**, **Mootha VK**, **Mukherjee S**, **Ebert BL**, **Gillette MA**, **Paulovich A**, **Pomeroy SL**, **Golub TR**, **Lander ES**, **Mesirov JP.** Gene set enrichment analysis: A knowledge-based approach for interpreting genome-wide expression profiles. *Proc Natl Acad Sci* 102: 15545–15550, 2005. doi:10.1073/pnas.0506580102.
44. **Mootha VK**, **Lindgren CM**, **Eriksson K-F**, **Subramanian A**, **Sihag S**, **Lehar J**, **Puigserver P**, **Carlsson E**, **Ridderstråle M**, **Laurila E**, **Houstis N**, **Daly MJ**, **Patterson N**, **Mesirov JP**, **Golub TR**, **Tamayo P**, **Spiegelman B**, **Lander ES**, **Hirschhorn JN**, **Altshuler D**, **Groop LC.** PGC-1α-responsive genes involved in oxidative phosphorylation are coordinately downregulated in human diabetes. *Nat Genet* 34: 267–273, 2003. doi:10.1038/ng1180.
45. **Hinman SS**, **Wang Y**, **Kim R**, **Allbritton NL.** In vitro generation of self-renewing human intestinal epithelia over planar and shaped collagen hydrogels. *Nat Protoc* 16: 352–382, 2021. doi:10.1038/s41596-020-00419-8.
46. **Sato T**, **Stange DE**, **Ferrante M**, **Vries RGJ**, **Van Es JH**, **Van den Brink S**, **Van Houdt WJ**, **Pronk A**, **Van Gorp J**, **Siersema PD**, **Clevers H.** Long-term expansion of epithelial organoids from human colon, adenoma, adenocarcinoma, and Barrett's epithelium. *Gastroenterology* 141: 1762–1772, 2011. doi:10.1053/j.gastro.2011.07.050.
47. **Wang Y**, **Kim R**, **Hwang S-HJ**, **Dutton J**, **Sims CE**, **Allbritton NL.** Analysis of interleukin 8 secretion by a stem-cell-derived human-

intestinal-epithelial-monolayer platform. *Anal Chem* 90: 11523–11530, 2018. doi:10.1021/acs.analchem.8b02835.

48. **Maciel AAFL**, **Oriá RB**, **Braga-Neto MB**, **Braga AB**, **Carvalho EB**, **Lucena HBM**, **Brito GAC**, **Guerrant RL**, **Lima AAM.** Role of retinol in protecting epithelial cell damage induced by Clostridium difficile toxin A. *Toxicon* 50: 1027–1040, 2007. doi:10.1016/j.toxicon.2007.07.010.
49. **Henkel D**, **Tatge H**, **Schöttelndreier D**, **Tao L**, **Dong M**, **Gerhard R.** Receptor binding domains of TcdB from *Clostridioides difficile* for chondroitin sulfate proteoglycan-4 and frizzled proteins are functionally independent and additive. *Toxins* 12: 736, 2020. doi:10.3390/toxins12120736.
50. **Song L**, **Zhao M**, **Duffy DC**, **Hansen J**, **Shields K**, **Wungjiranirun M**, **Chen X**, **Xu H**, **Leffler DA**, **Sambol SP**, **Gerding DN**, **Kelly CP**, **Pollock NR.** Development and validation of digital enzyme-linked immunosorbent assays for ultrasensitive detection and quantification of *Clostridium difficile* toxins in stool. *J Clin Microbiol* 53: 3204–3212, 2015. doi:10.1128/JCM.01334-15.
51. **Burclaff J**, **Bliton RJ**, **Breau KA**, **Cotton MJ**, **Hinesley CM**, **Ok MT**, **Sweet CW**, **Zheng A**, **Bankaitis ED**, **Ariel P**, **Magness ST.** SOX9 elongates cell cycle phases and biases fate decisions in human intestinal stem cells (Preprint). *bioRxiv*, 2022. doi:10.1101/2022.11.03.514885.
52. **Fanning AS**, **Ma TY**, **Anderson JM.** Isolation and functional characterization of the actin-binding region in the tight junction protein ZO-1. *FASEB J* 16: 1835–1837, 2022. doi:10.1096/fj.02-0121fje.
53. **Schindelin J**, **Arganda-Carreras I**, **Frise E**, **Kaynig V**, **Longair M**, **Pietzsch T**, **Preibisch S**, **Rueden C**, **Saalfeld S**, **Schmid B**, **Tinevez J-Y**, **White DJ**, **Hartenstein V**, **Eliceiri K**, **Tomancak P**, **Cardona A.** Fiji: an open-source platform for biological-image analysis. *Nat Methods* 9: 676–682, 2012. doi:10.1038/nmeth.2019.
54. **Pothoulakis C**, **Gilbert RJ**, **Cladaras C**, **Castagliuolo I**, **Semenza G**, **Hitti Y**, **Montcrief JS**, **Linevsky J**, **Kelly CP**, **Nikulasson S**, **Desai HP**, **Wilkins TD**, **Lamont JT.** Rabbit sucrase-isomaltase contains a functional intestinal receptor for *Clostridium difficile* toxin A. *J Clin Invest* 98: 641–649, 1996. doi:10.1172/JCI118835.
55. **Papatheodorou P**, **Carette JE**, **Bell GW**, **Schwan C**, **Guttenberg G**, **Brummelkamp TR**, **Aktories K.** Lipolysis-stimulated lipoprotein receptor (LSR) is the host receptor for the binary toxin *Clostridium difficile* transferase (CDT). *Proc Natl Acad Sci USA* 108: 16422–16427, 2011. doi:10.1073/pnas.1109772108.
56. **Van Beers EH**, **Buller HA**, **Grand RJ**, **Einerhand AW**, **Dekker J.** Intestinal brush border glycohydrolases: structure, function, and development. *Crit Rev Biochem Mol Biol* 30: 197–262, 1995. doi:10.3109/10409239509085143.
57. **Just I**, **Selzer J**, **Wilm M**, **Eichel-Streiber CV**, **Mann M**, **Aktories K.** Glucosylation of Rho proteins by *Clostridium difficile* toxin B. *Nature* 375: 500–503, 1995. doi:10.1038/375500a0.
58. **Just I**, **Wilm M**, **Selzer J**, **Rex G**, **Von Eichel-Streiber C**, **Mann M**, **Aktories K.** The enterotoxin from *Clostridium difficile* (ToxA) monoglucosylates the rho proteins. *J Biol Chem* 270: 13932–13936, 1995. doi:10.1074/jbc.270.23.13932.
59. **Just I**, **Fritz G**, **Aktories K**, **Giry M**, **Popoff MR**, **Boquet P**, **Hegenbarth S**, **von Eichel-Streiber C.** Clostridium difficile toxin B acts on the GTP-binding protein Rho. *J Biol Chem* 269: 10706–10712, 1994.
60. **Vancamelbeke M**, **Vanuytsel T**, **Farré R**, **Verstockt S**, **Ferrante M**, **Van Assche G**, **Rutgeerts P**, **Schuit F**, **Vermeire S**, **Arijs I**, **Cleynen I.** Genetic and transcriptomic bases of intestinal epithelial barrier dysfunction in inflammatory bowel disease. *Inflamm Bowel Dis* 23: 1718–1729, 2017. doi:10.1097/MIB.0000000000001246.
61. **Suzuki T.** Regulation of the intestinal barrier by nutrients: the role of tight junctions. *Anim Sci J* 91: e13357, 2020. doi:10.1111/asj.13357.
62. **Kowalczyk MS**, **Tirosh I**, **Heckl D**, **Rao TN**, **Dixit A**, **Haas BJ**, **Schneider RK**, **Wagers AJ**, **Ebert BL**, **Regev A.** Single-cell RNA-seq reveals changes in cell cycle and differentiation programs upon aging of hematopoietic stem cells. *Genome Res* 25: 1860–1872, 2015. doi:10.1101/gr.192237.115.
63. **Srinivasan B**, **Kolli AR**, **Esch MB**, **Abaci HE**, **Shuler ML**, **Hickman JJ.** TEER measurement techniques for in vitro barrier model systems. *SLAS Technol* 20: 107–126, 2015. doi:10.1177/2211068214561025.
64. **Van Der Flier LG**, **Clevers H.** Stem cells, self-renewal, and differentiation in the intestinal epithelium. *Annu Rev Physiol* 71: 241–260, 2009. doi:10.1146/annurev.physiol.010908.163145.
65. **Chandrasekaran R**, **Lacy DB.** The role of toxins in Clostridium difficile infection. *FEMS Microbiol Rev* 41: 723–750, 2017. doi:10.1093/femsre/fux048.
66. **Nusrat A**, **von Eichel-Streiber C**, **Turner JR**, **Verkade P**, **Madara JL**, **Parkos CA.** Clostridium difficile toxins disrupt epithelial barrier function by altering membrane microdomain localization of tight junction proteins. *Infect Immun* 69: 1329–1336, 2001. doi:10.1128/IAI.69.3.1329-1336.2001.
67. **Yu H**, **Chen K**, **Sun Y**, **Carter M**, **Garey KW**, **Savidge TC**, **Devaraj S**, **Tessier ME**, **von Rosenvinge EC**, **Kelly CP**, **Pasetti MF**, **Feng H.** Cytokines are markers of the *Clostridium difficile*-induced inflammatory response and predict disease severity. *Clin Vaccine Immunol* 24: e00037, 2017. doi:10.1128/CVI.00037-17.
68. **Odenwald MA**, **Turner JR.** Intestinal permeability defects: is it time to treat? *Clin Gastroenterol Hepatol* 11: 1075–1083, 2013. doi:10.1016/j.cgh.2013.07.001.
69. **Gibson GR**, **Whitacre EB**, **Ricotti CA.** Colitis induced by nonsteroidal anti-inflammatory drugs. Report of four cases and review of the literature. *Arch Intern Med* 152: 625–632, 1992.
70. **Suissa D**, **Delaney JAC**, **Dial S**, **Brassard P.** Non-steroidal anti-inflammatory drugs and the risk of Clostridium difficile-associated disease. *Br J Clin Pharmacol* 74: 370–375, 2012. doi:10.1111/j.1365-2125.2012.04191.x.
71. **Permpalung N**, **Upala S**, **Sanguankeo A**, **Sornprom S.** Association between NSAIDs and *Clostridium difficile*-associated diarrhea: a systematic review and meta-analysis. *Can J Gastroenterol Hepatol* 2016: 7431838, 2016. doi:10.1155/2016/7431838.
72. **Bhatt AP**, **Gunasekara DB**, **Speer J**, **Reed MI**, **Pena AN**, **Midkiff BR**, **Magness ST**, **Bultman SJ**, **Allbritton NL**, **Redinbo MR.** Nonsteroidal anti-inflammatory drug-induced leaky gut modeled using polarized monolayers of primary human intestinal epithelial cells. *ACS Infect Dis* 4: 46–52, 2018. doi:10.1021/acsinfecdis.7b00139.
73. **Niu X**, **De Graaf IAM**, **Langelaar-Makkinje M**, **Horvatovich P**, **Groothuis GMM.** Diclofenac toxicity in human intestine ex vivo is not related to the formation of intestinal metabolites. *Arch Toxicol* 89: 107–119, 2015. doi:10.1007/s00204-014-1242-6.
74. **Kararli TT.** Comparison of the gastrointestinal anatomy, physiology, and biochemistry of humans and commonly used laboratory animals. *Biopharm Drug Dispos* 16: 351–380, 1995. doi:10.1002/bdd.2510160502.
75. **McConnell EL**, **Fadda HM**, **Basit AW.** Gut instincts: explorations in intestinal physiology and drug delivery. *Int J Pharm* 364: 213–226, 2008. doi:10.1016/j.ijpharm.2008.05.012.
76. **Dong L**, **Tomassen MM**, **Ariëns RMC**, **Oosterink E**, **Wichers HJ**, **Veldkamp T**, **Mes JJ**, **Govers C.** Clostridioides difficile toxin A-mediated Caco-2 cell barrier damage was attenuated by insect-derived fractions and corresponded to increased gene transcription of cell junctional and proliferation proteins. *Food Funct* 12: 9248–9260, 2021. doi:10.1039/d1fo00673h.
77. **Pietrangeli P**, **Corpetti C**, **Seguella L**, **Del Re A**, **Pesce M**, **Vincenzi M**, **Lori C**, **Annunziata G**, **Mateescu MA**, **Sarnelli G**, **Esposito G**, **Marcocci L.** Lathyrus sativus diamine oxidase reduces Clostridium difficile toxin A-induced toxicity in Caco-2 cells by rescuing RhoA-GTPase and inhibiting pp38-MAPK/NF-κB/HIF-1α activation. *Phytother Res* 35: 415–423, 2021. doi:10.1002/ptr.6814.
78. **Natoli M**, **Leoni BD**, **D'Agnano I**, **Zucco F**, **Felsani A.** Good Caco-2 cell culture practices. *Toxicol In Vitro* 26: 1243–1246, 2012. doi:10.1016/j.tiv.2012.03.009.
79. **Hidalgo IJ**, **Raub TJ**, **Borchardt RT.** Characterization of the human colon carcinoma cell Line (Caco-2) as a model system for intestinal epithelial permeability. *Gastroenterology* 96: 736–749, 1989.
80. **Mao EJ**, **Kelly CR**, **Machan JT.** Racial differences in clostridium difficile infection rates are attributable to disparities in health care access. *Antimicrob Agents Chemother* 59: 6283–6287, 2015. doi:10.1128/AAC.00795-15.
81. **Pollock NR.** Ultrasensitive detection and quantification of toxins for optimized diagnosis of *Clostridium difficile* infection. *J Clin Microbiol* 54: 259–264, 2016. doi:10.1128/JCM.02419-15.
82. **Mileto SJ**, **Jardé T**, **Childress KO**, **Jensen JL**, **Rogers AP**, **Kerr G**, **Hutton ML**, **Sheedlo MJ**, **Bloch SC**, **Shupe JA**, **Horvay K**, **Flores T**, **Engel R**, **Wilkins S**, **McMurrick PJ**, **Lacy DB**, **Abud HE**, **Lyras D.** Clostridioides difficile infection damages colonic stem cells via TcdB, impairing epithelial repair and recovery from disease. *Proc Natl Acad Sci U S A* 117: 8064–8073, 2020. doi:10.1073/pnas.1915255117.

83. **Mahida YR**, **Makh S**, **Hyde S**, **Gray T**, **Borriello SP.** Effect of *Clostridium difficile* toxin A on human intestinal epithelial cells: induction of interleukin 8 production and apoptosis after cell detachment. *Gut* 38: 337–347, 1996. doi:10.1136/gut.38.3.337.
84. **Hansen A**, **Alston L**, **Tulk SE**, **Schenck LP**, **Grassie ME**, **Alhassan BF**, **Veermalla AT**, **Al-Bashir S**, **Gendron F-P**, **Altier C**, **Macdonald JA**, **Beck PL**, **Hirota SA.** The P2Y6 receptor mediates *Clostridium difficile* toxin-induced CXCL8/IL-8 production and intestinal epithelial barrier dysfunction. *PLoS One* 8: e81491, 2013. doi:10.1371/journal.pone.0081491.
85. **Branka J**, **Vallette G**, **Jarry A**, **Bou-Hanna C**, **Lemarre P**, **Van P**, **Laboisse C.** Early functional effects of *Clostridium difficile* toxin A on human colonocytes. *Gastroenterology* 112: 1887–1894, 1997. doi:10.1053/gast.1997.v112.pm9178681.
86. **Johal SS**, **Solomon K**, **Dodson S**, **Borriello SP**, **Mahida YR.** Differential effects of varying concentrations of *Clostridium* difficile toxin A on epithelial barrier function and expression of cytokines. *J Infect Dis* 189: 2110–2119, 2004. doi:10.1086/386287.
87. **Dostert C**, **Grusdat M**, **Letellier E**, **Brenner D.** The TNF family of ligands and receptors: communication modules in the immune system and beyond. *Physiol Rev* 99: 115–160, 2019. doi:10.1152/physrev.00045.2017.
88. **Koon HW**, **Wang J**, **Mussatto CC**, **Ortiz C**, **Lee EC**, **Tran DH-N**, **Chen X**, **Kelly CP**, **Pothoulakis C.** Fidaxomicin and OP-1118 inhibit clostridium difficile toxin A- and B-mediated inflammatory responses via inhibition of NF-κB activity. *Antimicrob Agents Chemother* 62: e01513–e01517, 2018. doi:10.1128/AAC.01513-17.
89. **Matte I**, **Lane D**, **Côté E**, **Asselin A-E**, **Fortier L-C**, **Asselin C**, **Piché A.** Antiapoptotic Proteins Bcl-2 and Bcl-X_L inhibit *Clostridium difficile* toxin A-induced cell death in human epithelial cells. *Infect Immun* 77: 5400–5410, 2009. doi:10.1128/IAI.00485-09.
90. **Speelman P**, **Butler T**, **Kabir I**, **Ali A**, **Banwell J.** Colonic dysfunction during cholera infection. *Gastroenterology* 91: 1164–1170, 1986. doi:10.1016/s0016-5085(86)80012-9.
91. **Field M.** Intestinal ion transport and the pathophysiology of diarrhea. *J Clin Invest* 111: 931–943, 2003. doi:10.1172/JCI18326.